THE ASTROPHYSICAL JOURNAL, 383:380–400, 1991 December 10

NON-LTE MODELS OF TITAN'S UPPER ATMOSPHERE

ROGER V. YELLE
Lunar and Planetary Laboratory, 9th Floor, Gould-Simpson Building, University of Arizona, Tucson, AZ 85721
Received 1991 March 18; accepted 1991 June 18

ABSTRACT

Models for the thermal structure of Titan's upper atmosphere, between 0.1 mbar and 10^{-2} nbar are presented. The calculations include non-LTE heating/cooling in the rotation-vibration bands of CH_4, C_2H_2, and C_2H_6, absorption of solar IR radiation in the near-IR bands of CH_4 and subsequent cascading to the ν_4 band of CH_4, absorption of solar EUV and UV radiation, thermal conduction and cooling by HCN rotational lines. Unlike earlier models, the calculated exospheric temperature agrees well with observations, because of the importance of HCN cooling. The calculations predict a well-developed mesopause with a temperature of 135–140 K at an altitude of approximately 600 km and pressure of ~ 0.1 μbar. The mesopause is at a higher pressure than predicted by earlier calculations because non-LTE radiative transfer in the rotation-vibration bands of CH_4, C_2H_2, and C_2H_6 is treated in an accurate manner. The accuracy of the LTE approximation for source functions and heating rates is discussed. It found that C_2H_6 acts as a heat source near the mesopause by absorbing radiation from the warm stratosphere; consequently, the temperature at the mesopause depends sensitively on the C_2H_6 abundance. Because of the strong coupling between photochemistry and thermal structure the agreement between calculated and observed temperatures lend support to the photochemical model of Yung et al.

Subject headings: planets: satellites — planets: Saturn

1. INTRODUCTION

It is convenient to divide Titan's atmosphere into four regions: the troposphere, stratosphere, mesosphere, and thermosphere. The troposphere has a negative temperature gradient and encompasses the region between the surface and the tropopause at ~ 130 mbar. The stratosphere extends from the tropopause to 1 mbar, is in radiative equilibrium and has a positive temperature gradient due largely to absorption of solar radiation by aerosols. The mesosphere begins at 1 mbar and, according to the results reported here, has a negative temperature gradient, leading to a well-developed, cold mesopause at 0.1 μbar, which represents the base of the thermosphere. The negative temperature gradient is caused by radiative cooling-to-space in the rotation-vibration bands of several hydrocarbons. The thermosphere extends from the mesopause to the exobase at 10^{-2} nbar and has a modest (~ 40 K) temperature rise caused by solar EUV heating.

Physical models for the thermal structure of Titan's upper atmosphere have fallen into two categories, LTE radiative-convective models for the stratosphere and troposphere (Samuelson 1983; McKay, Pollack, & Courtin 1989) and thermal conduction models for the thermosphere (Friedson & Yung 1984; Lellouch et al. 1990). This paper presents the first calculations for the thermal structure in the mesosphere. A goal of this research has been to connect the thermosphere and mesosphere in a physically justifiable fashion; thus, comprehensive models for the entire upper atmosphere are presented and the region near the mesopause is particularly emphasized.

There is a significant amount of data available on Titan's upper atmosphere. A solar occultation observed by the Voyager ultraviolet spectrometer (UVS) measured the exospheric temperature at ~ 1265 km above the surface near the morning and evening terminators (Smith et al. 1982). Recent ground-based occultations have provided constraints on the thermal structure near 1 μbar and possibly at deeper pressures (Hubbard et al. 1991). Infrared observations made by *Voyager* have placed some firm constraints on the methane abundance and thermal structure in the stratosphere (Lellouch et al. 1989, 1990; Coustenis, Bezard, & Gautier 1989). Thus, there are observational constraints on thermal structure models at a number of different altitudes, allowing important tests of our understanding of energy balance in the upper atmosphere. In the near future, improvements in ground-based IR instrumentation hold promise for greatly improved spectral studies (Kostiuk et al. 1990), while the planned Cassini mission to the Saturn system should provide a many-fold increase in our knowledge of Titan's upper atmosphere. Theoretical guidance, supplied by the modeling approach presented here, is essential.

Although there are important observational constraints on Titan's thermal structure, our knowledge of Titan's upper atmosphere is really very limited. Complicating the situation is the lack of accurate information on some critical molecular parameters. One of the prime goals of this study is to pinpoint the critical data needed, both in the lab and on Titan, to better direct further research. Thus, although models are presented which satisfy available observational constraints, a more important result of this work is the identification of the processes and molecular species which control the thermal structure.

Studies of the thermal structure of the upper atmosphere have not met with much success. Friedson & Yung (1984) performed the first investigation and were able to reproduce the observed exospheric temperature. Unfortunately, this agreement was illusory because of an error in the calculation of solar heating rates. Lellouch et al. (1990) in a subsequent study calculated solar heating rates roughly a factor of 6 larger than the Friedson & Yung (1984) values and predicted exospheric temperatures nearly a factor of two larger than the observations. Lellouch et al. (1990) found that they could reproduce the

observed temperatures by using small heating efficiencies but this procedure is not physically motivated and is very unsatisfying because it conflicts with well-established heating efficiences in the terrestrial upper atmosphere (Lellouch et al. 1990).

An important contribution of the Lellouch et al. (1990) work is the determination of an empirical temperature-pressure profile. This profile satisfies the constraints imposed by infrared (Lellouch et al. 1989; Coustenis et al. 1989) and UV data (Smith et al. 1982) as well as hydrostatic equilibrium. Lellouch et al. (1990) infer a mean temperature of 160 K between 200 and 880 km, 169 K between 880 and 1115 km, and 180 K between 1115 and 1265 km. From this analysis Lellouch et al. (1990) conclude that Titan must have a cool mesopause near 800 km, to explain the low mean temperature.

The Lellouch et al. (1990) calculations did not include enough physics to model the mesosphere properly. The calculations presented here are far more sophsticated, resolve some of the earlier problems, and reveal some interesting aspects of energy balance in the upper atmosphere which have not been previously recognized. The models are able to reproduce the important constraints on Titan's thermal structure for reasonable values of the uncertain input parameters. This is surprising considering the abysmal failure of one-dimensional thermal models on many other planets (e.g., Venus, Jupiter, Saturn, Uranus, and Neptune) and adds to the importance of studies of Titan's upper atmosphere.

The models presented here cover eight decades of pressure and include a wide array of physical processes including solar heating in the UV and IR, thermal conduction, non-LTE cooling in the ν_4 band of CH_4, the ν_5 band of C_2H_2, and the ν_9 band of C_2H_6, coupling between the ν_4 band of CH_4 and higher vibrational levels, and cooling by rotational transitions in HCN. The models are one-dimensional and are designed to represent the global mean thermal structure. Dynamical processes on large and small scales are neglected, but the models may be used to study radiative forcing of tides caused by variations in solar isolation. The possibility of aerosol heating is also examined. The magnitude of aerosol heating is poorly constrained and definitive conclusions cannot be drawn without further observational or theoretical input. Sections 2–8 describe various aspects of the theoretical models; §§ 9 and 10 present and summarize the results.

2. NON-LTE COOLING IN VIBRATION-ROTATION BANDS

On Titan the significant, thermally active molecules in the upper atmosphere are CH_4, C_2H_2, C_2H_6 and HCN. CH_4, C_2H_2, and C_2H_6 affect the thermal structure through their vibrational bands at 1306 cm^{-1}, 729 cm^{-1} and 821 cm^{-1}. The HCN band at 713 cm^{-1} is not included in the work presented here because calculations indicate that its inclusion would change the computed temperature profile by less than 1 K; however, as discussed in § 7, the rotational transitions of the HCN molecule play a critical role in the thermal structure. Collisional excitation rates for the vibrational levels of the hydrocarbons are low in the upper atmosphere, and a non-LTE formulation must be used to determine the populations heating/cooling rates. The theory of non-LTE vibrational cooling is reviewed below.

Curtis & Goody (1956) presented the first thorough discussion of the theory behind non-LTE radiative cooling in a vibrational band and applied it to the 15 μm band of CO_2 in the terrestrial upper atmosphere. Subsequent investigations of CO_2 non-LTE in the terrestrial atmosphere were made by Houghton (1969), Kuhn & London (1969), Shved (1974), Dickinson (1972), Kutepov & Shved (1978), Apruzese & Strobel (1984), and Lopez-Puertas et al. (1986). Advances over the earlier work included improved band models, treatment of line shapes, efficient numerical techniques and inclusion of multiple vibrational levels of the CO_2 molecule. Reviews of these developments in terrestrial atmospheric science are given by Dickinson (1984). Dickinson (1972, 1975, 1976) applied CO_2 non-LTE theory to Venus and in subsequent work (Dickinson & Ridley 1977) was able to predict many aspects of upper atmospheric dynamics on that planets. CH_4 non-LTE processes in the upper atmospheres of the outer planets have been examined by Appleby (1990).

A completely general formulation of the non-LTE problem is very complex and all of the works mentioned above make use of some approximations to simplify the problem. However, none of the previous studies employ the set of approximations which are appropriate for Titan; therefore, the theory of non-LTE in a vibrational band is revisited below and a simple but useful form for vibrational band source functions in Titan's atmosphere is derived.

A major simplification made in the following discussion is the neglect of stimulated emissions. This assumption is well justified at the cold temperatures in outer solar system atmospheres. The stimulated emission factors $[1 - \exp(-h\nu/kT)]$ at 175 K for the CH_4 band at 1306 cm^{-1}, the C_2H_2 band at 729 cm^{-1} and the C_2H_6 band at 821 cm^{-1} are 0.99998, 0.997, 0.9990, respectively.

Another common simplification, that the extent of the vibrational band is small compared to the frequency scale of the Planck function, is not justified. This is particularly true for the ν_4 band of CH_4 which covers several hundred wavenumbers. Although most of the opacity is concentrated near the band center at 1306 cm^{-1}, this spectral region is also very optically thick, which greatly diminishes the radiative cooling rate. As a consequence, much of the cooling occurs in the optically thin wings of the band where the Planck function differs significantly from its value at band center. Figure 1 demonstrates this. The absorption coefficient falls rapidly beyond ~ 50 cm^{-1}

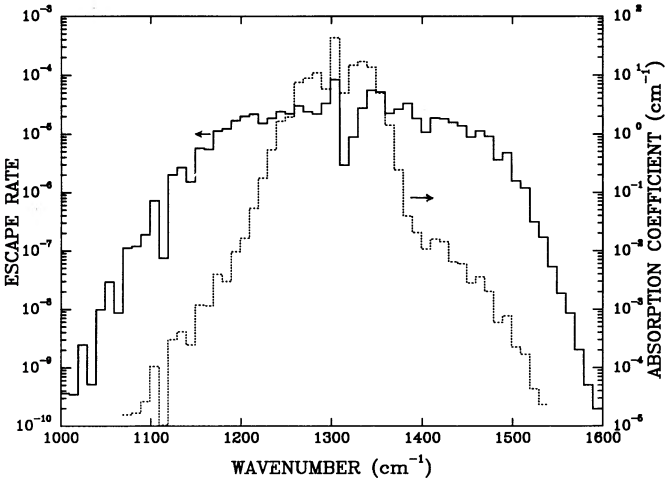

FIG. 1.—Overhead escape rate for a thermal source and the absorption coefficient for the ν_4 band of CH_4. The calculations are based on the model atmosphere of Lellouch et al. (1990) at a presssure of 100 μbar. Photons escape the atmosphere over a range of roughly 400 cm^{-1}

from the band center but photons escape over a much larger range of wavenumbers. The escape rate plotted in this figure is defined as

$$E(\nu) = \frac{\int_{\Delta\nu} dvk_\nu \exp(-\tau_\nu)}{\int dvk_\nu}, \quad (1)$$

where k_ν is the volume absorption coefficient and τ_ν the monochromatic optical depth. The frequency integration in the numerator is over a 10 cm^{-1} spectral region centered on ν while the frequency integration in the denominator is over the full extent of the band. $E(\nu)$ represents, in an approximate way, the relative contributions to the cooling rate from different frequency intervals. Clearly it is necessary to include frequencies at least 200 cm^{-1} from the band center to properly calculate source functions, heating rates and other important quantities. The Planck function at 175 K changes by more than an order of magnitude over this large a frequency range.

2.1. *Source Functions*

If stimulated emissions are neglected, the source function is given by

$$\mathcal{S}_\nu = \frac{2h\nu^3}{c^2}\frac{w_0 N_1}{w_1 N_0}, \quad (2)$$

where N_1 and N_0 are the densities of molecules in the vibrationally excited and ground state, respectively. The quantities w_1 and w_0 are the statistical weights of the upper and lower vibrational states. Derivation of equation (2) also relies on the assumptions that the rotational levels of the upper and lower vibrational states are in LTE, that the emission of radiation from the upper level is isotropic and that the spectral line profiles for emission and absorption are identical and uncorrelated. All of these conditions are satisfied in the upper atmosphere of Titan.

In general, an excited vibrational level is populated by collisional excitation of ground state molecules, absorption of radiation and energy transfer from other vibrationally excited states, and is depopulated by collisions, spontaneous emissions and vibrational energy transfer. In the absence of significant transport processes for the excited molecules (which is easy to show), the density of excited states must be in statistical equilibrium and

$$\frac{N_1}{N_0} = \frac{B_{01}\mathcal{J} + C_{01} + D_1}{A_{10} + C_{10}}, \quad (3)$$

where C_{01} and C_{10} are the excitation and de-excitation rates due to collisions with the ambient atmosphere. The quantity A_{10} is the Einstein coefficient for spontaneous emission from the excited state, while B_{01} is the Einstein coefficient for absorption and is related to the frequency integral of the absorption coefficient, $k_o(z) = \int dvk_\nu$ through

$$\frac{h\nu}{4\pi} B_{01} = \frac{k_o(z)}{N_0(z)}. \quad (4)$$

The quantity $\mathcal{J}$ is the mean intensity of the band defined by

$$\mathcal{J}(z) = \frac{1}{2k_o(z)} \int dvk_\nu(z) \int_{-1}^{1} d\mu \mathcal{J}_\nu(\mu, z). \quad (5)$$

It is also useful to define a mean Planck function through

$$\mathcal{B}(z) = \frac{1}{k_o(z)} \int dvk_\nu(z)\mathcal{B}_\nu(z), \quad (6)$$

where $\mathcal{B}_\nu$ is the Planck function, and a mean source function

$$\mathcal{S}(z) = \frac{1}{k_o(z)} \int dvk_\nu(z)\mathcal{S}_\nu(z). \quad (7)$$

The quantity D_1 is included in equation (3) to account for excitation of the low-lying fundamentals through vibrational energy transfer from higher vibrational levels. In Titan's upper atmosphere this cascade of vibrational quanta is driven by the absorption of solar near-IR radiation. The D_1 term is discussed in more detail below. De-excitation of the low-lying fundamentals through energy transfer to other vibrationally excited states is negligible on Titan and is not included in equation (3).

The excitation and de-excitation rates for collisional and radiative processes may be related through detailed balancing arguments to yield the following relations:

$$\bar{N}_0 C_{01} = \bar{N}_1 C_{10} \quad (8)$$

and

$$w_1 \bar{N}_0 B_{01} \mathcal{B} = w_0 \bar{N}_1 A_{10}, \quad (9)$$

where the overbar on the densities indicates their LTE values. Substitution of equations (3), (7), and (8) into (2) yields

$$\frac{\mathcal{S}_\nu}{\mathcal{B}_\nu} = \frac{\mathcal{J} + \theta}{\mathcal{B}(1+\epsilon)} + \frac{\epsilon}{1+\epsilon}, \quad (10)$$

where $\epsilon \equiv C_{10}/A_{10}$ and

$$\theta \equiv \frac{D_1}{4\pi B_{01}}. \quad (11)$$

Equation (10) shows that the source function has the same frequency dependence as the Planck function. This is a direct result of the assumption of rotational LTE.

Most of the work on CO_2 non-LTE has assumed that the band width is small compared to the frequency scale of the Planck function (see Kuhn 1969; Dickinson 1972; Lopez-Puertas et al. 1986). The form of the source function used in those works may be obtained from equation (10) with the substitution $\mathcal{B}_\nu = \mathcal{B}$. Curtis & Goody (1956) in the original work on CO_2 and Appleby (1990) in his work on CH_4 non-LTE on the outer planets retain the frequency dependence of the Planck function but ignore interactions between vibration levels. Setting $\Theta = 0$ in equation (10) gives a form for the source function which is equivalent to that used by those authors.

2.2. *Collisional De-Excitation Rates*

It is evident from equation (10) that the non-LTE source function depends critically on the ϵ parameter, which in turn depends on the collisional deactivation rate C_{10}. Unfortunately, our knowledge of the collisional deactivation rates is far from adequate, especially at low temperatures.

Collisional deactivation of an excited state converts vibrational energy into translational energy (heat) and is often referred to as a V-T transition. The collisional de-excitation rate, C_{10}, for a V-T transition is related to the de-excitation probability, P_{10}, through

$$C_{10} = ZN_a P_{10}, \quad (12)$$

where N_a is the atmospheric density and the collision rate, Z, is given by

$$Z = \sigma^2 \sqrt{(8\pi kT/\mu)}, \quad (13)$$

where σ is the collision diameter and μ is the reduced mass.

The value of P_{10} depends on the relative velocity of the colliding molecules and consequently on the temperature of the gas. Usually values for P_{10} are measured at temperatures near 300 K or higher, rather than the low temperatures which are more relevant for studies of atmospheres on outer solar system bodies. Several previous studies (Strobel & Smith 1973; Friedson & Yung 1984; Lellouch et al. 1990) have employed the Landau-Teller formula (Landau & Teller 1936) to extrapolate room temperature measurements to lower temperatures,

$$P_{10}(T) = A \exp(-b/T^{1/3}) . \quad (14)$$

Lellouch et al. (1990) use a value of $b = 35$ K$^{1/3}$ for CH_4 and C_2H_2 collisions with N_2, which implies a factor of 3 decrease in P_{10} from 300 to 175 K.

The temperature dependence implied by the Landau-Teller formula is likely to be incorrect. Schwartz, Slawsky, & Herzfeld (1952, hereafter SSH) in a more rigorous study of V-T transitions found that an additional temperature dependence enters through the dependence of P_{10} on the energy of the vibrational state, $h\nu$, and derived the following expression:

$$P_{10}(T) = A \exp(-b/T^{1/3}) \exp(h\nu/2kT) . \quad (15)$$

The SSH theory specifies the constant b,

$$b = 3\left(\frac{2\pi^4\mu\nu^2}{\alpha^2 k}\right)^{1/3} , \quad (16)$$

where μ is the reduced mass for the collision and α is an inverse length scale for the interaction potential. Like the Landau-Teller expression, equaton (15) is a high temperature approximation which should only be used if

$$T \gg T_c \equiv \frac{h\alpha}{2\pi^2 k}\sqrt{2h\nu/\mu} . \quad (17)$$

Table 1 lists calculations of T_c based on equation (17) and shows that the high temperature approximation should be adequate for C_2H_2 and C_2H_6, but is questionable for CH_4.

Further complicating the problem is the issue of vibration-rotation (V-R) collisions. There is evidence that the transfer of energy from vibrational to rotational excitation is important, particularly for polyatomic molecules (Cotrell & McCoubrey 1961). Attempts to account for energy flow to the rotational degree of freedom through simple modifications of the SSH theory have met with some success. One procedure followed is to alter the definition of reduced mass in equation (16) through

$$\frac{1}{\mu} = \frac{1}{m_1} + \frac{1}{m_2} + \frac{A_1 d_1^2}{I_1} + \frac{A_2 d_2^2}{I_2} , \quad (18)$$

where $m_{1,2}$ are the molecular masses, $I_{1,2}$ moments of inertia and $d_{1,2}$ internuclear distances. The parameters $A_{1,2}$ depend on the details of the collision but have typical values of 0.25 (Zittell & Moore 1973).

Table 1 lists calculations of b based on equations (16) and (18). Lellouch et al. (1990) determined a value of $b = 35$ K$^{1/3}$ for C_2H_4 by fitting the measurement of Yuan et al. (1973) to the Landau-Teller formula (15). On the other hand, calculations based on equations (16) and (18) imply a value of $b = 135$ K$^{1/3}$. The discrepancy is resolved if the Yuan et al. (1973) data is fitted to equation (16), to account for the exp ($h\nu/2kT$) factor. This procedure gives a value of $b = 137$ K$^{1/3}$, in excellent agreement with the modified SSH theory. Agreement for other molecules is not as good. For example, Zittel & Moore (1973) find that the observed temperature dependence of P_{10} for CH_4—Ar collisions is weaker than implied by the modified SSH theory. Similarly, low temperature measurements of the CO_2–N_2 de-excitation rate (Allen et al. 1980) predict values of b which are in poor agreement with SSH calculations. Nevertheless, the agreement between theory and experiment for C_2H_4 is encouraging and the modified SSH theory can at least be used to indicate the magnitude of P_{10} temperature variations in an approximate way. The last column in Table 1 lists the value of P_{10} at 175 K extrapolated from room temperature on the basis of the modified SSH theory.

3. VIBRATIONAL CHEMISTRY

In addition to the uncertainties associated with extrapolation of rate coefficients to low temperatures discussed in the last section, the vibrational populations of the low-lying fundamentals are also affected by interactions with other vibrational states. Laboratory data on the de-excitation rates and the complications introduced by vibration-vibration (V-V) transitions are discussed in the following subsections.

3.1. *Methane*

The time constant for de-excitation of the ν_4 level by N_2–CH_4 collisions at room temperature has been measured by Yardley, Fertig, & Moore (1970), who infer a deactivation probability at room temperature of $P_{10} = 5.5 \times 10^{-6}$. Yardley et al. (1970) determine the de-excitation probability by monitoring the decay rate of laser-induced fluorescence. Their experiments were performed with CH_4 mole fractions from 2% to 10%. Wang & Springer (1977), determine the de-excitation probability by measuring the dispersion of ultrasonic sound waves in a CH_4–N_2 mixture. The Wang & Springer (1977) measurements were performed with CH_4 mole fractions of 95%, 90% and 70%. Extrapolations of the Wang & Springer (1977) measurements to smaller values of the CH_4 mole fraction gave results in agreement with the Yardley et al. (1970) measurements.

Vibration-vibration transfer also plays an important role in the thermal interactions between CH_4 and the radiation field because absorption of solar photons in the near-IR bands at 3.3, 2.3, and 1.7 μm, and subsequent cascading through V-V collisions, help populate the ν_4 level. Table 2 lists the important vibrational bands for CH_4, C_2H_2 and C_2H_6. The CH_4 bands naturally separate into groups with an overtone of the ν_4 band

TABLE 1

V–T De-Excitation Probabilities

Transition	α(Å^{-1})	μ(amu)	T_c(K)	b(K$^{1/3}$)	P_{10} (300 K)	P_{10} (175 K)
CH_4–N_2	4.66	4.42	198	125	5.5×10^{-6}	1.4×10^{-6}
C_2H_2–N_2	4.43	7.38	123	104	1.25×10^{-4}	2.1×10^{-5}
C_2H_6–N_2	4.32	5.06	123	101	1.25×10^{-4}	2.1×10^{-5}

TABLE 2

MOLECULAR BAND PARAMETERS

Molecule	Band	ν(cm^{-1})	S(cm^2 cm^{-1})	A (s^{-1})
CH_4	ν_4	1306	5.42×10^{-18}	2.12
3.3 μm	$2\nu_4$	2610		
	$\nu_2 + \nu_4$	2828		
	ν_1	2914	1.15×10^{-17}	4.24
	ν_3	3019		
	$2\nu_2$	3072		
2.3 μm	$3\nu_4$	3914		
	$\nu_2 + 2\nu_4$	4123		
	$\nu_1 + \nu_4$	4224	7.4×10^{-19}	6.36
	$\nu_3 + \nu_4$	4313		
	$\nu_2 + \nu_3$	4546		
1.7 μm	$4\nu_4$	5128		
	$\nu_3 + 2\nu_4$	5585		
	$\nu_1 + \nu_2 + \nu_4$	5775	2.1×10^{-20}	8.48
	$\nu_2 + \nu_3 + \nu_4$	5861		
	$2\nu_3$	6005		
C_2H_2	ν_5	729	2.35×10^{-17}	4.75
C_2H_6	ν_9	821	5.74×10^{-19}	0.37

as the lowest energy member in any one group. The transfer of energy within a group caused by CH_4–CH_4 collisions has been studied by Yardley & Moore (1968) and Hess, Kung, & Moore (1980), while Hess & Moore (1976) studied V-V processes in CH_4–rare gas mixtures. Unfortunately there does not appear to be any work on V-V processes induced by CH_4–N_2 collisions; nevertheless, some general conclusions can be drawn and some estimates made.

Yardley & Moore (1968) and Hess et al. (1980) studied V-V transfer through laser excitation of the ν_3 and $2\nu_3$ states. Measurement of the decay rates of various fluorescence emission were analyzed to determine the rate constants. The V-V processes are found to be three to four orders of magnitude more rapid than V-T processes. For example, Hess et al. (1980) find that conversion of a ν_3 quanta into two bending quanta ($2\nu_4$, $2\nu_2$, or $\nu_2 + \nu_4$) has a probability of 2×10^{-2}, compared to 7×10^{-6} for deactivaton of the ν_4 level by CH_4–Ar collisions. Consequently, the energy absorbed into the ν_3 state is not converted directly into translational energy but is either transferred to bending modes or re-emitted as radiation. Only deactivation of CH_4 by H_2 violates this rule, presumably because of the low mass of the H_2 molecule. Because Ar and N_2 deactivate the ν_4 level of CH_4 at nearly the same rate, a V-V probability of 2×10^{-2} is adopted for relaxation from higher vibrational levels within a group to the ν_4 overtone level.

Solar energy absorbed in the 3.3, 2.7, and 2.3 μm bands is eventually channeled into thermal energy, hot band radiation, or excitation of the ν_4 level. Heating occurs as a result of the initial V-V collision and through subsequent V-T transitions between the ν_4 overtones. As Table 2 indicates, photons absorbed in the near-IR bands typically have energies larger than the closest ν_4 overtone. The energy difference between the vibrational level which absorbs the photon and the closest ν_4 overtone is released as heat in a V-V collision.

Once the ν_4 overtone is excited further heating may occur through collisionally induced V-V transitions between overtone levels. If, on the other hand, the overtone level is de-excited by radiative decay, energy escapes the atmosphere as hot band radiation. Both collisional and radiative decay of the overtone levels eventually produce one quanta of fundamental ν_4 excitation. The fraction of the energy absorbed in the 3.3, 2.3, and 1.7 μm bands which is converted in thermal energy, hot band radiation, or ν_4 excitation can be calculated as follows. For definiteness consider excitation of the ν_3 state. Define Q_ν as the excitation rate due to the absorption of solar energy,

$$Q_\nu(z) = \tfrac{1}{2} k_\nu \pi \mathscr{F}_\nu \int_0^1 d\mu \exp(-\tau_\nu/\mu) \tag{19}$$

where $\pi\mathscr{F}_\nu$ is the solar flux and τ_ν is the monochromatic optical depth. The factor of $\frac{1}{2}$ is included for diurnal averaging. Further define ϵ_3 and ϵ_4 as the ratio of the ν_3 and ν_4 collisional de-excitation rate to the radiative decay rate. The energy which subsequently appears as excitation of the bending modes is $2h\nu_4 \epsilon_3/(1 + \epsilon_3)$, while $h(\nu_3 - 2\nu_4)$ appears as heat. A fraction equal to $\epsilon_4/(1 + \epsilon_4)$ of the energy deposited in the $2\nu_4$ is channeled into translational modes by collisional de-excitation. If instead a radiative transition occurs the energy is lost from the atmosphere as hot band radiation. Collecting all the terms, the heating rate caused by absorption of solar radiation followed by V-V cascading is given by

$$Q_{3.3} = \frac{\epsilon_3}{1 + \epsilon_3} \int_{\text{band}} d\nu \left(\frac{\nu - 2\nu_4}{\nu} + \frac{\epsilon_4}{1 + \epsilon_4} \frac{\nu_4}{\nu} \right) Q_\nu . \tag{20}$$

The heating rate caused by absorption in the 2.3 μm band is given by

$$Q_{2.3} = \int_{\text{band}} d\nu \left(\frac{\nu - 3\nu_4}{\nu} + \frac{2\epsilon_4}{1 + \epsilon_4} \frac{\nu_4}{\nu} \right) Q_\nu , \tag{21}$$

while the heating rate caused by absorption in the 1.7 μm band is given by

$$Q_{1.7} = \int_{\text{band}} d\nu \left(\frac{\nu - 4\nu_4}{\nu} + \frac{3\epsilon_4}{1 + \epsilon_4} \frac{\nu_4}{\nu} \right) Q_\nu . \tag{22}$$

The 2.3 μm and 1.7 μm bands are absorbed fairly deep in the atmosphere where the V-V collision rate is much larger than the radiative decay rate therefore the efficiency factor in front of the integral has been set to 1. It is also assumed that the ratio of V-T de-excitation to radiative decay for overtone bands is equal to that for the fundamental, thus the $\epsilon_4/(1 + \epsilon_4)$ factor applies to each step in the cascade.

The rate at which the ν_4 level is excited by the cascade process is

$$D_1 = \frac{\epsilon_3}{1 + \epsilon_3} \int_{\text{band}} d\nu \frac{\nu_4}{\nu} Q_\nu . \tag{23}$$

which holds for all three of the CH_4 near-IR bands. Equation (23) expresses the fact that absorption of a quantum of ν_3 radiation followed by a V-V transition eventually leads to the deposition of one quantum of vibrational excitation in the ν_4 state.

Expressions (20), (21), and (22) differ from those presented by Appleby (1990). Appleby's expressions include a term for heat released by collisional de-excitation of the ν_4 level, which is more properly included through the Θ term in equation (10).

3.2. *Acetylene*

Relaxation of the ν_5 level of C_2H_2 has been studied by Haeger et al. (1980) and Haeger, Krieger, & Pfab (1981) by observing the time decay of fluorescence from the ν_5 state after excitation of the $\nu_2 + \nu_4 + \nu_5$ state. The inferred de-activation probability at room temperature is $P_{10} = 1.25 \times 10^{-4}$. This analysis has been criticized by Smith, David, & Smith (1985) who argue that the rate limiting step could be the

$\nu_2 + \nu_4 + \nu_5 \rightarrow \nu_5$ transition, and the measured fluorescence signals may reflect this rate rather than the rate for de-excitation of the ν_5 state. If true, the actual value for the ν_5 de-activation probability could be larger than the value quoted above.

Relaxation of the ν_5 level is further complicated by the presence of the IR inactive ν_4 level at 621 cm^{-1}. Collisional transfers between the two levels is rapid because of the small energy difference. Even though the ν_4 level is radiatively inactive, the cooling rates may be affected because the presence of the ν_4 level could alter the population of the ν_5 level. Let N_0 represent the density of ground state molecules, N_1 the density of molecules in the ν_4 state, and N_2 the density in the ν_5 state. If the interaction of radiation with the ν_4 state is neglected N_1 may be eliminated from the equations of statistical equilibrium with the result

$$\frac{N_2}{N_0} = \frac{B_{02}\mathscr{J} + C_{02} + C_{12}C_{01}/(C_{12} + C_{10})}{A_{20} + C_{20} + C_{21}C_{10}/(C_{12} + C_{10})}, \quad (24)$$

where again A_{20}, $B_{02}\mathscr{J}$ and C_{ij} represent the spontaneous decay rate, the absorption rate, and the collisional transfer rates: the subscripts indicate the direction of energy flow. Substitution of equation (24) into equation (2) gives

$$\frac{\mathscr{S}_\nu}{\mathscr{B}_\nu} = \frac{\mathscr{J}}{\mathscr{B}(1+\tilde{\epsilon})} + \frac{\tilde{\epsilon}}{1+\tilde{\epsilon}}, \quad (25)$$

where

$$\tilde{\epsilon} = \frac{\tilde{C}_{20}}{A_{20}}, \quad (26)$$

and

$$\tilde{C}_{20} = C_{20} + \frac{C_{12}C_{10}}{C_{12} + C_{10}} \exp(\Delta E/kT), \quad (27)$$

where ΔE is the energy separation between ν_5 and ν_4 states. Thus, the equation for the source function takes the same form as that for a two-level system. It is interesting to examine limiting values for $\tilde{C}_{20}$. If $C_{12} \gg C_{10}$ and $\Delta E \ll kT$ then

$$\tilde{C}_{20} = C_{20} + C_{10}, \quad (28)$$

which expresses the fact that collisional transfer between the 1 and 2 levels is so rapid that it does not slow down the loss of vibrational quanta. Collisional de-excitation of the 1 and 2 levels play an equal role in the problem and the transfer of energy of translation depends on the net rate for creating ground state molecules. If, on the other hand, $C_{10} \gg C_{12}$, then

$$\tilde{C}_{20} = C_{20} + C_{21}, \quad (29)$$

and the heating rate depends only on the rate at which quanta are lost from the 2 level.

The collisional rates C_{12} or C_{21} have not been measured individually but this is hardly important. The laser fluorescence techniques for measuring the ν_5 deactivation rate, determines this rate by monitoring the time decay of fluorescence from the state in question after excitation of an upper state. In essence what is measured is the rate at which quanta are lost from the ν_5 state: the measurements do not discriminate between loss the ν_4 level or ground state. The experiments measure the value of $\tilde{C}_{20}$ rather than C_{20}, and the data may be used directly in our calculations. However, equation (27) also demonstrates that the coupling between the ν_5 and ν_4 levels introduces an additional temperature dependence into the collisional de-excitation rate. The exponential in equation (27) increases by a factor of 2.6 from 300 to 175 K, and may offset the decrease in collisional de-excitation rates predicted by the SSH theory.

Lellouch et al. (1990) attempted to account for the presence of the ν_4 level by doubling the statistical weight of the ν_5 state. The discussion above demonstrates that this procedure is incorrect and their cooling rates are too high.

3.3. *Ethane*

Very little is known about collisional de-excitation of the C_2H_6 band at 821 cm^{-1}. Some early attempts to infer relaxation times from specific heat measurements found very large de-excitation probabilities for C_2H_6–C_2H_6 collisions, $P_{10} \sim 10^{-2}$ (Lambert & Salter 1959; Valley & Levgold 1960). The Lambert & Salter (1955) measurements of the C_2H_2 de-excitation probability are orders of magnitude larger than the more recent measurements by Haeger et al. (1981). However, even if $P_{10} = 10^{-2}$ for C_2H_6–C_2H_6 collisions, as the Lambert & Salter (1959) measurements indicate, the de-excitation rate for C_2H_6–N_2 collision may be much less rapid. For example, the C_2H_2–C_2H_2 de-excitation probability is an order of magnitude larger than the C_2H_2–N_2 de-excitation probability (Haeger et al. 1980, 1981). On the other hand, deactivation of C_2H_6 may be very different from C_2H_2 because C_2H_6 has a torsional vibration mode at 275 cm^{-1} with overtones at 520 cm^{-1} and possibly 725 cm^{-1} (Herzberg 1945). If de-excitation occurs through these states it may be rapid relative to C_2H_2. As the CH_4 data indicate, V-V transitions between closely lying states tend to be far more rapid than V-T transitions. This suggests that the de-excitation rate for the ν_9 band of C_2H_6 could plausibly be much more rapid than the C_2H_2 de-excitation rate. Accurate laboratory measurements are required to solve the problem. Both slow and rapid de-excitation for C_2H_6 are considered in the following.

4. ABSORPTION COEFFICIENTS

Determination of the non-LTE mean intensity or source function requires integration of the product of specific intensity and absorption coefficient over the extent of the band (eq. [5]). This is a difficult computational problem because a typical band may extend over several hundred wavenumbers while the absorption coefficient and specific intensity vary on the scale of the Doppler width of $\sim 10^{-3}$ cm^{-1}; thus, hundreds of thousands of frequency points must be considered.

In several previous studies of non-LTE effects the absorption calculations have been simplified by neglecting overlap of spectral lines (Dickinson 1972; Lopez-Puertas et al. 1986). This allows the binning of lines in groups with an average line strength and subsequent use of line transfer functions to solve the radiative transfer problem. Unfortunately, this approximation is completely unacceptable for the problem considered here. Figure 2 shows that errors on the order of 20% are introduced into the overhead escape function (eq. [1]) by the neglect of overlap. Errors in the heating rate should be of the same order. Overlapping spectral lines can be handled with random band models (see Goody & Yung 1989). However, band models require extensive testing to determine the size of the errors introduced by the band model simplifications and are difficult to use in inhomogeneous atmospheres. The spectral mapping transformations (SMTs) recently introduced by West, Chen, & Crisp (1990) avoid these difficulties.

Conceptually, SMTs are simply a shuffling of frequencies

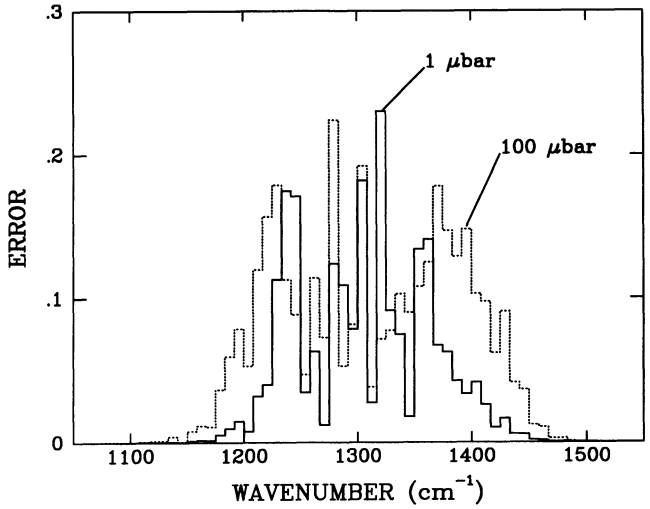

FIG. 2.—Error introduced into the overhead escape rate by neglecting overlap of closely spaced spectral lines. The calculations are based on the Lellouch et al. (1990) model atmosphere at pressures of 1 and 100 μbar. The error is defined as the difference between an isolated line calculation and the calculation including overlap divided by the overlap calculation.

and absorption coefficients inside a spectral bin (which must be small compared to the spectral scale of the Planck function) into an order which is easy to integrate, and subsequent grouping of frequencies with similar absorption coefficients into smaller divisions. An average absorption coefficient is defined for each group and it is these average coefficients which are used to solve the radiative transfer equation. It is necessary to insure that the frequencies are grouped in exactly the same manner at each altitude step to maintain the integrity of vertical (optical depth) integrations inherent in solutions of the radiative transfer equation. Once this is accomplished, each spectral group will contain frequencies which have similar absorption coefficients at all altitudes. Thus, calculation of atmospheric transmission with SMTs is an exact method, in the sense that the only approximation is related to the tolerance used to decide if a certain frequency fits into a given bin. West et al. (1990) propose two methods for grouping frequencies into bins. The calculations presented here use an algorithm based on their method II.

To calculate an SMT the transmission at each frequency is compared with the average transmission for a spectral group for every atmospheric layer. The frequency is included in the group if the transmissions agree to within a specified tolerance in every layer. This has the effect of grouping together all frequencies which are very optically thin ($T \sim 1$) and all frequencies which are very optically thick ($T \sim 0$) even if their absorption coefficients vary widely.

Line parameters for CH_4 and C_2H_2 are taken from the GEISA tape (Husson 1986). Line parameters for C_2H_6 were derived from the work of Daunt et al. (1984). Throughout most of Titan's upper atmosphere the absorption lines are well described by Doppler profiles; however, at the highest pressures considered here (0.1 to 1 mbar) collisional broadening becomes important and Voigt profiles are used throughout the atmosphere. Numerical tests indicate that results for pure Doppler profiles differ by 40% at 1 mbar and 15% at 0.1 mbar from results with Voigt profiles. Absorption coefficients are assumed to be zero at distances greater than 300 Lorentz widths from line center. The behavior of the absorption coefficient in the far wings of pressure broadened lines is not well known but this has little effect on the absorption properties of an upper atmosphere. Test calculations performed with a cutoff at 1000 Lorentz widths yielded temperature profiles which differed by less than 0.1 K from calculations with a cutoff of 300 Lorentz widths.

Figure 3 shows the absorption spectrum and associated SMTs for the ν_4 band of methane in the 1290–1300 cm^{-1} region at three different pressure levels in the Lellouch et al. (1990) model of Titan's atmosphere. By nature, though, the SMTs depend on the variation of temperature with pressure throughout the entire upper atmosphere. A tolerance of 20% is used for this and subsequent calculations. Only 17 frequency bins are required to accurately represent the transmission properties of this region of the spectrum. Savings of this magnitude are typical. For example, accurate calculations for the entire $CH_4\nu_4$ band require approximately 300,000 frequency integration points. SMTs calculated with the Lellouch et al. (1990) model atmosphere, divided into 51 layers from 0.1 mbar to 0.01 nbar, reduce this number to 411.

The SMTs used here are designed to reproduce the transmission properties of the atmosphere to perfect accuracy for a flat input spectrum. Comparison of SMT and line-by-line transmissions confirms this expectation. On the other hand, the heating rate depends not only on the average transmission but also on the average of the product of absorption coefficient and transmission. To further investigate the accuracy of SMTs, Figure 4 shows a comparison of the transmission for a thermal source defined by

$$T_\nu = \frac{\int_{\Delta\nu} d\nu k_\nu \exp(-\tau_\nu)}{\int_{\Delta\nu} d\nu k_\nu} \tag{30}$$

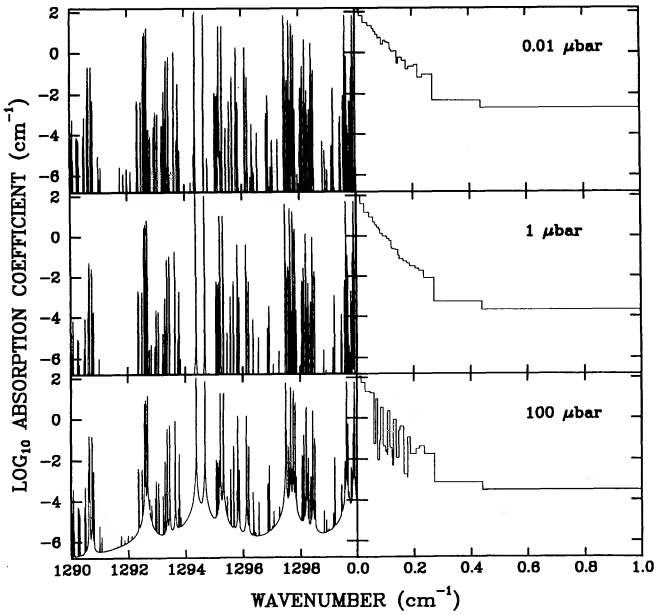

FIG. 3.—Absorption cross section of the ν_4 band of CH_4 from 1290 to 1300 cm^{-1} at three pressure levels in Titan's atmosphere (*left*) and the associated spectral mapping transformations (*right*). Although the wavenumber scale for the SMTs has the same extent as the spectra (i.e., 10 cm^{-1}) only the region from 0 to 1 cm^{-1} is shown because the region from 1 to 10 cm^{-1} contains a small number of bins representing the low opacity, optically thin spectral regions. Seventeen spectral regions are needed to represent the absorption properties of the 1290–1300 cm^{-1} region.

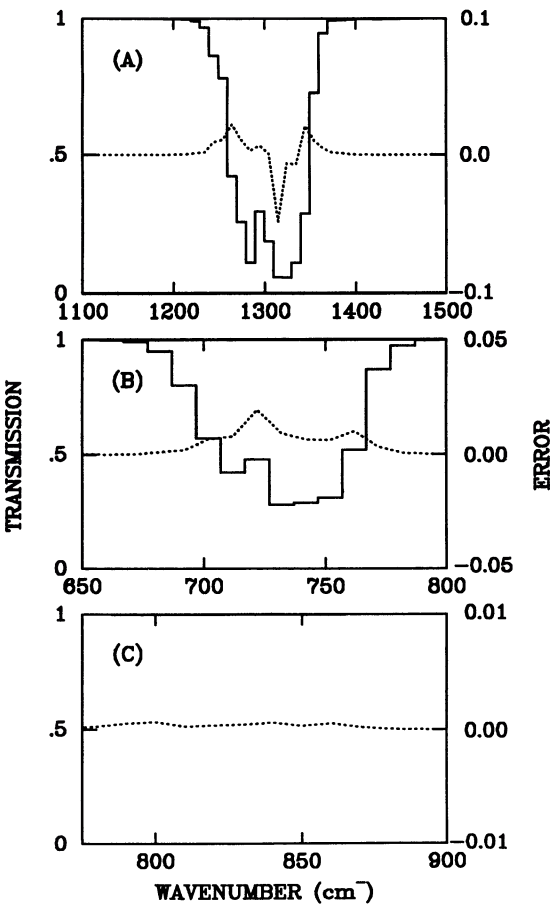

FIG. 4.—(*a*) Solid curve shows the overhead transmission ($\mu = 1$) of the atmosphere for a thermal source at 10 μbar for the ν_4 band of CH_4. The dotted curve shows the error in this quantity caused by use of SMTs rather than a line-by-line calculation. (*b*) Same as Fig. 4*a* for the ν_5 band of C_2H_2. (*c*) Same as Fig. 4*a* for the ν_9 band of C_2H_6. This band is optically thin and the transmission is unity throughout Titan's upper atmosphere.

for the SMT and line-by-line methods for CH_4, C_2H_2, and C_2H_6. The integrations cover a spectral region of 10 cm^{-1} centered about ν. The maximum error found for this case is less than 5% for CH_4, 1% for C_2H_2 and less than 0.1% for C_2H_6 (which is optically thin throughout the upper atmosphere). These calculations strongly suggest that the errors introduced into the heating rates through use of SMTs are very small.

5. RADIATIVE TRANSFER

CH_4 and C_2H_2 emissions are optically thick throughout the mesophere (i.e., 300 to 700 km). The strongest CH_4 lines have strengths of 10^{-19} cm^2 cm^{-1}, and optical depths at line center greater than 10^4 at 0.1 mbar. Similarly, the strongest C_2H_2 lines have strengths of 10^{-18} cm^2 cm^{-1}, and optical depths at line center $\sim 10^3$ at 0.1 mbar. Figure 4 demonstrates that Titan's atmosphere even at 1 μbar is opaque to a thermal source of photons near the center of the CH_4 and C_2H_2 bands. The transmission functions shown in Figure 4 are calculated for the vertical; the transmission along oblique rays will be much smaller. C_2H_6, on the other hand, is optically thin throughout the upper atmosphere.

The radiative transfer equation must be solved to determine the intensities, source functions and heating rates for these bands. In differential form the radiative transfer equation is

$$\mu \frac{d\mathcal{I}_\nu}{d\tau_\nu} = \mathcal{I}_\nu - \mathcal{S}_\nu . \tag{31}$$

The source function $\mathcal{S}_\nu$ depends on the specific intensity $\mathcal{I}_\nu$ at each frequency within the band through equation (10). Thus, the set of radiative transfer equations at each frequency is coupled and must be solved simultaneously. Rybicki's method (see Mihalas 1978) is well suited to this problem because the computing time scales linearly with the number of frequency points. Rybicki's method also avoids other types of approximations (such as the Curtis-Godson approximation for inhomogeneous atmospheres) which are required when band models are used. The implementation of Rybicki's method for non-LTE radiative transfer in a molecular band is described in the Appendix.

While the differential form of the radiative transfer equation is preferred for numerical solutions, it is easier to gain physical insight from the integral form of the radiative transfer equation. Formal integration of the transfer equation coupled with equations (5)–(7) and (10) leads to

$$\mathcal{S} = \frac{1}{1+\epsilon}\left[\epsilon\mathcal{B} + \mathcal{B}_o + \int_{z_o}^{-\infty} dz' \mathcal{S}(z')\Lambda(z, z')\right] \tag{32}$$

where z_o is the altitude of the lower boundary,

$$\mathcal{B} = \tfrac{1}{2}\int d\nu k_\nu(z)\mathcal{B}_\nu(z_o)E_2[\tau_\nu(z, z_o)] \tag{33}$$

and

$$\Lambda(z, z') = \frac{1}{2k_o\mathcal{B}(z')}\int d\nu k_\nu(z)k_\nu(z')\mathcal{B}_\nu(z')E_1[\tau_\nu(z, z')] . \tag{34}$$

The quantity $\tau_\nu(z, z')$ is the monochromatic optical depth from z to z' and is defined to be positive. The three terms in equation (32) represent collisional excitation at altitude z, excitation by absorption of radiation from the lower boundary and excitation by radiative exchange with other altitudes. Cascading from higher vibrational levels has been neglected for the moment. In an optically thick situation $\Lambda(z, z')$ is sharply peaked near $z = z'$ and the equation is approximately satisfied if $\mathcal{S}$ is taken outside the integral, leading to

$$\mathcal{S} = \frac{\epsilon\mathcal{B} + \mathcal{B}_o}{\epsilon + X(z)} \tag{35}$$

where

$$X(z) = 1 - \int_{z_o}^{-\infty} dz'\Lambda(z, z') . \tag{36}$$

This estimate of the non-LTE source function is similar to the familiar cooling-to-space approximation for heating rates. Houghton (1986) presents a similar equation (his eq. [5.37]) which is derived in a more intuitive fashion. The advantage of this approach is that it clearly shows what assumptions are required to derive equation (35).

If the non-LTE–LTE transition point is defined as the location where $\mathcal{S} = 0.5\mathcal{B}$, equation (35) gives a simple criterion for the breakdown of LTE: $X(z) = \epsilon$. When $X(z)$ is small, because the optical depth is large and photons cannot readily escape to space, LTE will hold to small values of ϵ. This point has been made by Dickinson (1972), Houghton (1986), and Coustenis et al. (1989). Multiple scattering of radiation allows more

opportunities for collisional de-excitation, helping to maintain a Boltzmann distribution of excited levels.

Equation (35) can also be used to estimate the non-LTE heating rate. The heating rate H, in a vibrational band is given by

$$H = 4\pi k_o(\mathscr{I} - \mathscr{S}), \tag{37}$$

which can be rewritten as

$$H = 4\pi k_o \epsilon(\mathscr{S} - \mathscr{B}) \tag{38}$$

or

$$H = 4\pi k_o \frac{\epsilon}{1+\epsilon}(\mathscr{I} - \mathscr{B}), \tag{39}$$

where again cascading has been neglected. Substituting equation (35) leads to

$$H = 4\pi k_o\left(\frac{\mathscr{B}_o}{\epsilon + X} - \frac{\epsilon X \mathscr{B}}{\epsilon + X}\right) \tag{40}$$

which is the cool-to-space approximation for the non-LTE heating rate. The net heating is the difference between energy absorbed from the lower boundary and energy escaping through the top and bottom boundaries. Equation (40) reduces to the LTE cool-to-space approximation at large values of ϵ and to the optically thin non-LTE cooling rate at small values of ϵ.

Equations (35) and (40) express the correct physics and qualitatively exhibit the proper behavior, but should not be trusted for quantitative calculations. The problem is that near $\epsilon = X$ the source function is changing most rapidly, violating the condition required to remove it from the integrand in equation (32). In an isothermal atmosphere, where variations in the source function are due solely to the breakdown of LTE, equation (35) will always overestimate the pressure of the $\mathscr{S} = 0.5\mathscr{B}$ point. Also, equation (35) does not apply in optically thin regions of the atmosphere because $\Lambda(z, z')$ is not sharply peaked at $z = z'$. Thus, equation (35) cannot be trusted to give a good approximation to the source functions at altitudes well above the non-LTE–LTE transition. Numerical calculations supporting these deduction are presented in § 9.

6. SOLAR ULTRAVIOLET HEATING

The heating rate due to absorption of solar UV radiation is calculated in a manner similar to that described by Lellouch et al. (1990) and similar results are obtained. Solar EUV fluxes are obtained from Torr & Torr (1985) for solar maximum and minimum. Solar Lyman alpha fluxes of 4×10^{11} and 2.3×10^{11} photon cm^{-2} s^{-1} are used for solar max and min, respectively. At wavelengths longward of 1216 Å the measurements of Mount & Rottman (1987) are used. The solar cycle variations in this spectral region are small and can be safely ignored.

The heating efficiency of solar EUV radiation is roughly 35% at Lyα and 70% in the EUV. These values are only rough estimates and more refined calculations, based on studies of the ionospheric chemistry are called for.

Figure 5 shows the heating rates for solar max and min along with the solar heating rate in the CH_4 near-IR bands for the Lellouch et al. (1990) model atmosphere. Absorption of UV radiation dominates above 500 km and IR radiation below. The results reported here are in good agreement with those calculated by Lellouch et al. (1990). An earlier calculation by Friedson & Yung (1984) obtained much lower rates and appears to be erroneous (Lellouch et al. 1990).

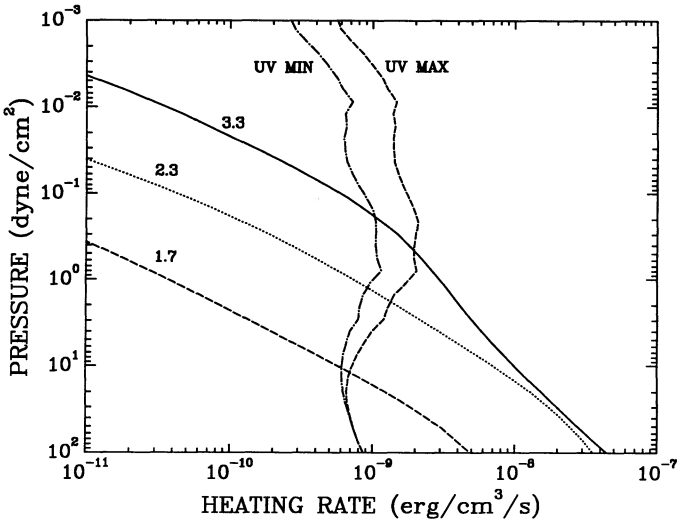

FIG. 5.—The heating rate in Titan's atmosphere due to absorption of solar UV and IR radiation, based on the Lellouch et al. (1990) model atmosphere. The curves labeled "UV MIN" and "UV MAX" refer to the heating rates at solar minimum and maximum, respectively. The other three curves represent the heating rate due to absorption of solar radiation in the 3.3, 2.3, and 1.7 μm bands. A deactivation probability of $P_{10} = 1.4 \times 10^{-6}$ is used in the calculations.

Heating by the EUV portion of the solar spectrum is dominated by the intense He II line at 304 Å, which is responsible for the peak 10^{-2} μbar. Deeper in the atmosphere, between 0.1 and 1 μbar, absorption of solar Lyα line by CH_4 dominates the heating. At still larger pressures solar UV radiation is absorbed predominantly by C_2H_2; however, over most of this range solar IR heating dominates. At the lowest pressures considered here the atmosphere is optically thin to UV radiation and the heating rate is proportional to the density. The constant of proportionality is 2.6×10^{-19} ergs s^{-1} molecule^{-1} for solar maximum and 1×10^{-19} ergs s^{-1} molecule^{-1} for solar minimum.

7. HCN ROTATIONAL COOLING

The hydrocarbon molecules discussed earlier do not possess permanent electric dipole moments; consequently, the transitions between rotational levels in the ground vibrational state are strongly forbidden. The same is true for N_2. HCN, however, is a linear asymmetric molecule and has a strong rotational line spectrum, with the potential to cause significant atmospheric cooling.

HCN is produced in the thermosphere as a byproduct of ionospheric chemistry and then flows downward to higher pressures. As a consequence the HCN mixing ratio is largest in the thermosphere and decreases with increasing pressure. There are no measurements of the HCN abundance in the thermosphere but photochemical calculations predict a mole fraction of $\sim 2 \times 10^{-3}$ (Yung, Allen, & Pinto 1984). The population of rotational levels should be in LTE throughout the upper atmosphere and non-LTE effects, which act to diminish cooling rates, will not apply. In addition the HCN rotational lines are optically thin and the cooling rate in the upper thermosphere will not be diminished by self absorption.

The importance of HCN cooling can be demonstrated fairly easily. In the optically thin limit the cooling rate, $-H$ is given

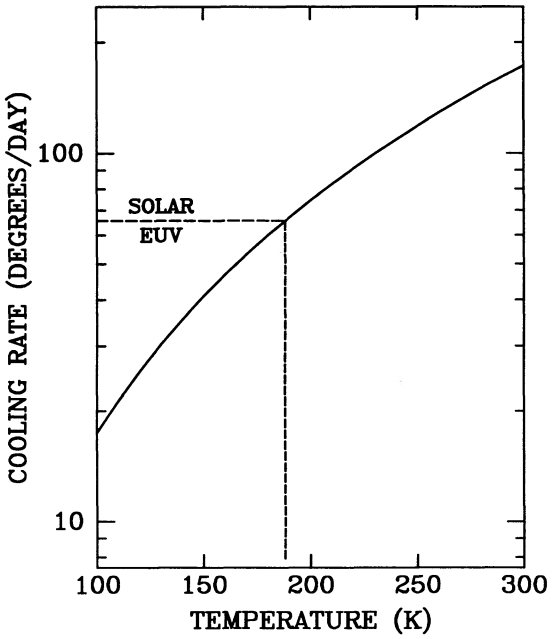

FIG. 6.—Approximate calculation of the HCN cooling rate in the upper thermosphere, assuming mole fraction of 1×10^{-3}. The horizontal line represents the solar EUV heating rate at solar maximum conditions and intersects the HCN curve at 187 K. This simple calculation illustrates that an approximate balance between HCN cooling and EUV heating is consistent with the observed exospheric temperature.

by

$$-H \simeq 4\pi \sum_j \mathscr{B}_{v_j} S_j N \tag{41}$$

where S_j is the strength of the jth rotational line and N the HCN number density. Figure 6 shows the cooling rate per HCN molecule calculated with equation (41) as a function of temperature. Also shown are the EUV heating rates per molecule for solar maximum. Using an HCN mole fraction of 1×10^{-3} and equating the HCN cooling rate to the solar max heating rate predicts an exospheric temperature of 187 K, which is within the range determined by the *Voyager* measurements (Smith et al. 1982).

In the calculations which follow, the HCN cooling rate is calculated with a line-by-line technique which takes full account of the optical depth and radiative transfer for each line. This more accurate treatment gives results which are in good agreement with the estimates made above in the upper reaches of the thermosphere. There is little doubt that the temperature of the thermosphere is controlled by HCN cooling, provided that the HCN abundance predicted by the photochemical models has the right order of magnitude.

8. THERMAL STRUCTURE CALCULATIONS

Collecting all the heating/cooling terms discussed above gives

$$\rho c_p \frac{dT}{dt} = \frac{r_o^2}{r^2} \kappa \frac{d}{dr} r^2 \frac{dT}{dr} + \sum_j H_j \tag{42}$$

where $\sum_j H_j$ represents the radiative heating terms, including solar UV and IR heating, non-LTE cooling by the hydrocarbon vibration-rotation bands and rotational cooling by HCN. The first term of the right-hand side of equation (42) represents energy transport by thermal conduction in a spherical atmosphere. The thermal conductivity, κ, is taken from Friedson & Yung (1984). There is a slight inconsistency here because the radiative transfer equation used to determine the heating rates for HCN and the hydrocarbons is solved in a plane parallel atmosphere. This approximation is made for convenience. It is simple to calculate the thermal conduction cooling rate in a spherical atmosphere but radiative transfer in a spherical atmosphere is horribly complex. Nevertheless, the plane parallel approximation should be accurate because only a small fraction of the total solid angle is influenced by curvature at any altitude.

Boundary conditions must be specified to complete the problem. The upper boundary is placed at a pressure of 10^{-5} μbar, which is roughly two scale heights below the exobase. The conductive heat flux is set to zero at this location. The energy carried away by evaporation from the top of the atmosphere is very small and may be ignored. The lower boundary is placed at 0.1 mbar. Calculations indicate that LTE is an excellent approximation at this pressure for all three hydrocarbons. The upward directed radiation field at the lower boundary is assumed to be described by a Planck function at 175 K. IRIS and RSS data indicate that the atmosphere between 0.1 and 10 mbar is nearly isothermal at this temperature (Lellouch et al. 1990) implying that this is an excellent approximation. Spectral regions with very low opacity may be influenced by emissions from the cool lower atmosphere but, because the opacity is low, these regions should have a negligible effect on the heating rates in the upper atmosphere.

Equation (42) is solved by a combined time-stepping, Newton-Raphson technique (Hastings & Roble 1977). The program stops when the sum of terms in the energy equation balance to within 1% of the largest term in the sum and temperature corrections have fallen below 0.1 K. Details of the numerical technique are described in the Appendix.

9. RESULTS

It is instructive to consider some simple cases to isolate non-LTE effects. To this end the behavior of source functions and heating rates in isothermal atmospheres with constant mixing ratios of CH_4, C_2H_2, and C_2H_6 are considered first, followed by calculations of the temperature profile, comparison with data and discussion of the relationship between thermal structure and photochemistry.

9.1. *Non-LTE Effects*

Figure 7 shows the source function for the v_4 band of CH_4 band without a cascade contribution (i.e., darkness), for cascade with an overhead sun, and for cascade with globally averaged insolation. A deactivation probability of 1.4×10^{-6} is used for all three calculations. The calculations without solar illumination show that the source function begins to depart appreciably from the Planck function at ~ 10 μbar and becomes half the Planck function at ~ 1.5 μbar where $\epsilon = 10^{-2}$. The cool-to-space approximation gives a much more rapid non-LTE–LTE transition and overestimates the pressure where $\mathscr{S} = 0.5\mathscr{B}$ by nearly a factor of 2. Cascading from higher vibrational levels enhances the source function by a small amount and tends to slow the departure from LTE. Although the effect of cascading on the source function is small, the consequences for the v_4 cooling rate are more appreciable: the cooling rates for darkness and an overhead sun differ by approximately 10% at 10 μbar.

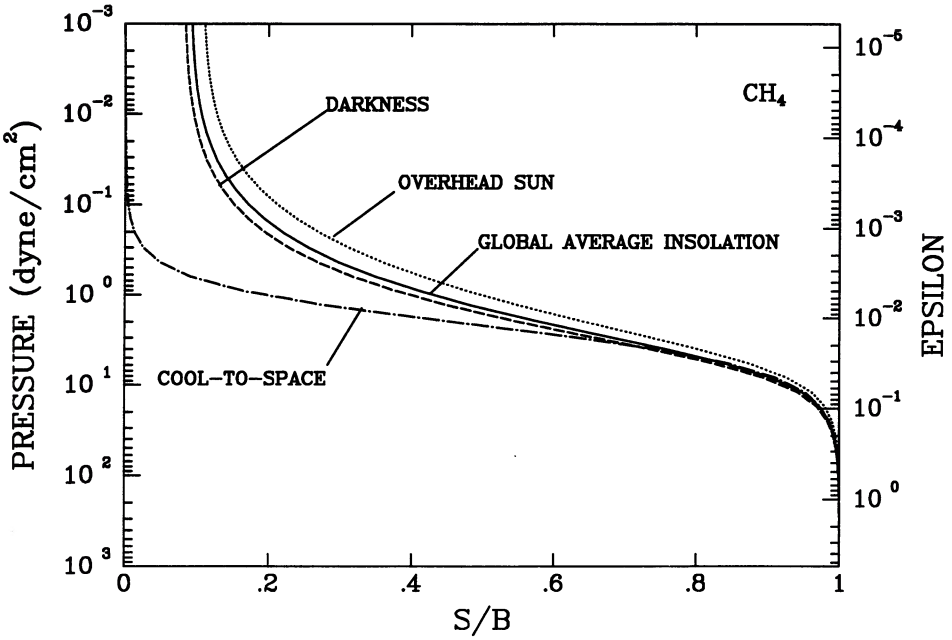

FIG. 7.—Ratio of source function to Planck function for the ν_4 band of CH_4 for three different illumination geometries. All calculations use a deactivation probability of $P_{10} = 1.4 \times 10^{-6}$. The model atmosphere used in the calculations is isothermal with a CH_4 mole fraction of 2%. Cascading of quanta from the near IR CH_4 bands to the ν_4 band enhances the source functions by about 10% for an overhead sun.

Previous thermal structure calculations of Titan's upper atmosphere have employed what can be called the "thermospheric" approximation. This approach was introduced by Chamberlain (1962) and has been employed in calculations of thermospheric structure for several atmospheres (Strobel & Smith 1973; Friedson & Yung 1984; Lellouch et al. 1990). The thermospheric approximation can be written as

$$H(z) = -\frac{4\pi\epsilon}{1+\epsilon} k_o \mathscr{B}(z) \qquad (43)$$

which is equivalent to the forms used by previous authors and shows clearly that the thermospheric approximation is equivalent to assuming that $\mathscr{J} \ll \mathscr{B}$ in equation (39). Generally this condition is well satisfied if the thermosphere is much hotter than the lower atmosphere and if the thermosphere is optically thin to IR radiation. The optically thin condition implies that most of the mean intensity, $\mathscr{J}$, originates in the cooler lower atmosphere and will reflect the value of the Planck function in that region, thus $\mathscr{J} \ll \mathscr{B}$. On Titan the temperature rise in the thermosphere is small, the optical depths are large, and the thermospheric approximation should be used with caution. The errors made with the thermospheric approximation for these simple atmospheres are on the order of 50%.

Figure 8 shows the non-LTE heating rates without cascading along with the LTE approximation, the "thermospheric" approximation and the cool-to-space approximation defined in equation (40). As expected, the LTE approximation is grossly inadequate at low pressures while the thermospheric approximation is grossly inadequate at high pressures. The transition region between the LTE and thermospheric asymptotes corresponds roughly to the altitude where the source function departs from LTE. There is an interesting enhancement of the non-LTE cooling rate above the LTE cooling rate which extends to relatively high pressures, despite the fact that the source function is very well approximated by the Planck function. This can be understood by examination of equation (38). Although $\mathscr{S}$ is nearly equal to $\mathscr{B}$ the heating rate is proportional to the product of ϵ and their difference. Because the heating rate is a small difference between two large but nearly equal numbers, even slight departures from LTE can have significant consequences. Physically speaking, the heating rate at high pressures is also affected by the source functions at low pressures, where departures from LTE are large. Consequently, the LTE approximation must be used more cautiously for heating rates than for source functions.

The cool-to-space approximation matches the LTE and thermospheric approximations at high and low pressures and does much better than either near 1 μbar where the LTE and thermospheric approximations are highly inaccurate. However, even the cool-to-space approximation is off by $\sim$50% in the 1 μbar regions, demonstrating that there is no substitute for an accurate non-LTE calculation.

Figure 9 shows C_2H_2 ν_5 source functions for two different values of the de-excitation probability. For $P_{10} = 2.1 \times 10^{-5}$ the source function begins to fall below its LTE value at $\sim$10 μbar and becomes equal to half the Planck function at 1.3 μbar, where $\epsilon = 5 \times 10^{-2}$. Because C_2H_2 is less abundant than CH_4 while their band strengths are similar one might expect that non-LTE effects would extend to higher pressures because radiation trapping is weaker, but the calculations demonstrate that radiation trapping is equally important. This happens because the C_2H_2 opacity is concentrated in a smaller spectral region than the CH_4 opacity causing the optical depths within the band to be relatively large.

Figure 10 shows the C_2H_2 non-LTE cooling rate along with the LTE, thermospheric and cool-to-space approximations. The situation is very similar to that described for CH_4. The non-LTE enhancement from 2 to 100 μbar is stronger for C_2H_2, probably because of the different nature of the spectral

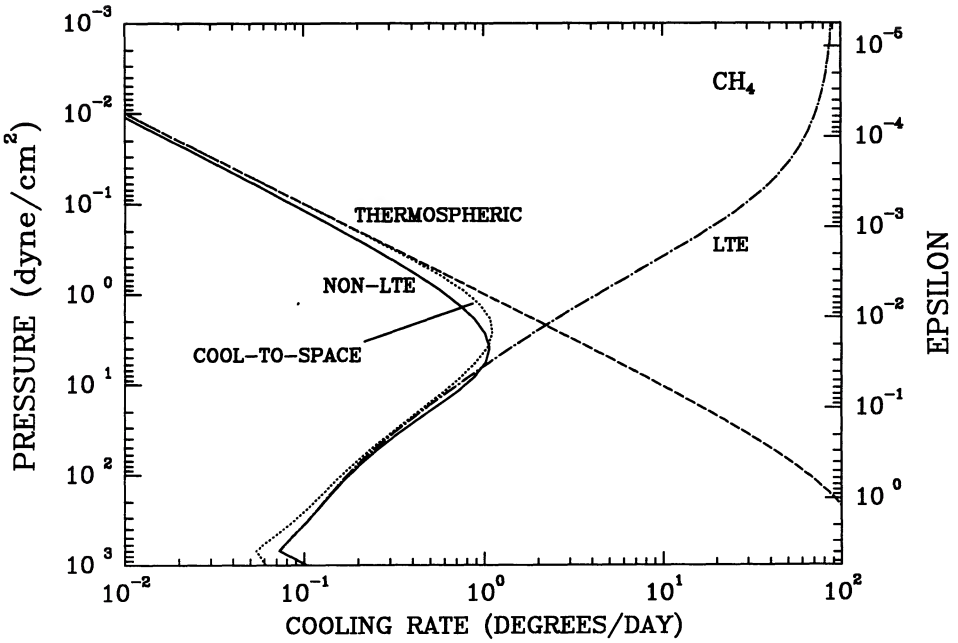

FIG. 8.—CH_4 cooling rate for the non-LTE calculations in this paper and two commonly used approximations. The calculations use a deactivation probability of $P_{10} = 1.4 \times 10^{-6}$. The model atmosphere used in the calculations is isothermal at 175 K with a CH_4 mole fraction of 2%. Cascading from higher vibrational states is not included. Although the thermospheric and LTE calculations have regions where they approach the non-LTE calculations both exhibit significant errors throughout the entire upper atmosphere.

line opacity distribution. Figures 11 and 12 show equivalent results for C_2H_6. The optical depth in the ν_9 band of C_2H_6 is small, and radiation trapping is unimportant. Consequently the source function shown in Figure 11 falls below the Planck function by $\sim 5\%$ near $\epsilon = 10$ at 30 μbar. Because the ν_9 band of C_2H_6 is optically thin, the cooling rate is proportional to the pressure at low altitudes and the square of pressure at high altitudes. Again the thermospheric approximation is $\sim 50\%$ too high at low pressures but is only slightly less accurate at high pressures because the optically thin approximation remains fairly accurate. The LTE approximation is proportional to pressure at all altitudes and departs from the

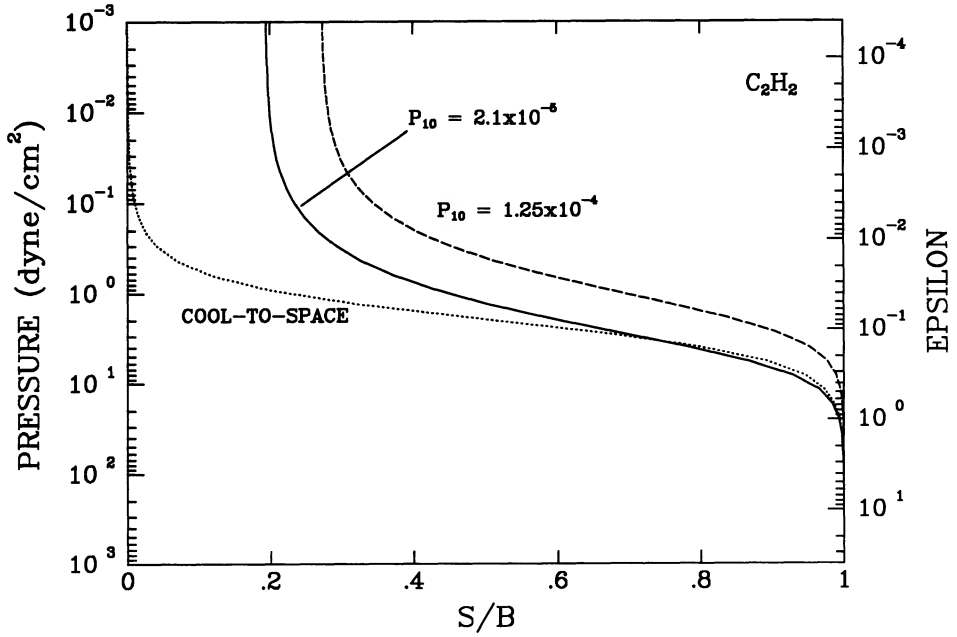

FIG. 9.—Ratio of source function to Planck function for the ν_5 band of C_2H_2 for two different values of the de-excitation probability. The vertical scale on the right-hand axis applies to the lower de-excitation probability. The model atmosphere used in the calculations is isothermal at 175 K with a C_2H_2 mole fraction of 0.01%.

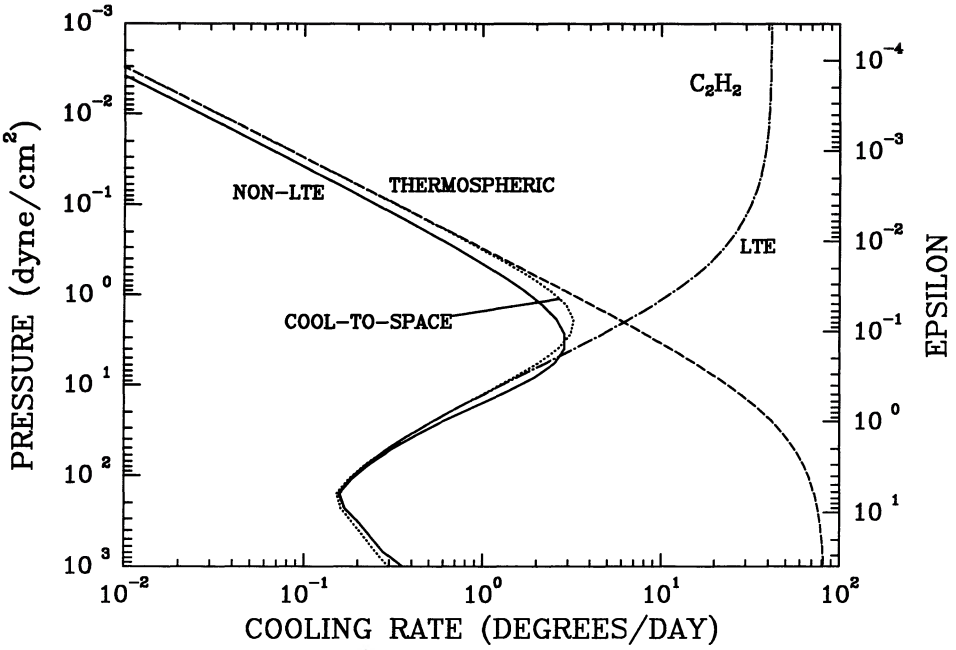

FIG. 10.—Cooling rates for the ν_5 band of C_2H_2. The calculations use a deactivation probability of $P_{10} = 2.1 \times 10^{-5}$. The model atmosphere used in the calculations is isothermal at 175 K with a C_2H_2 mole fraction of 0.01%.

non-LTE curve by 10% near 60 μbar where $\epsilon \simeq 15$, further demonstrating that radiation trapping is unimportant for this molecule.

9.2. *Thermal Structure*

Calculations of the thermal structure require a model for the altitude distribution of thermally active species. The calculations presented below use the results from a photochemical model (Yung et al. 1984, updated by M. Allen & Y. L. Yung 1989, personal communication). The densities of important species are shown in Figure 13. These calculations agree fairly well with values inferred from *Voyager* IRIS observations (Coustenis et al. 1989) in the stratosphere and *Voyager* UVS observations of the CH_4 abundance in the thermosphere. At the present time there are no measurements of the composition of Titan's mesosphere. The Yung and Allen calculations use the Lellouch et al. (1990) model atmosphere. In general the photochemical processes determining the abundance of minor

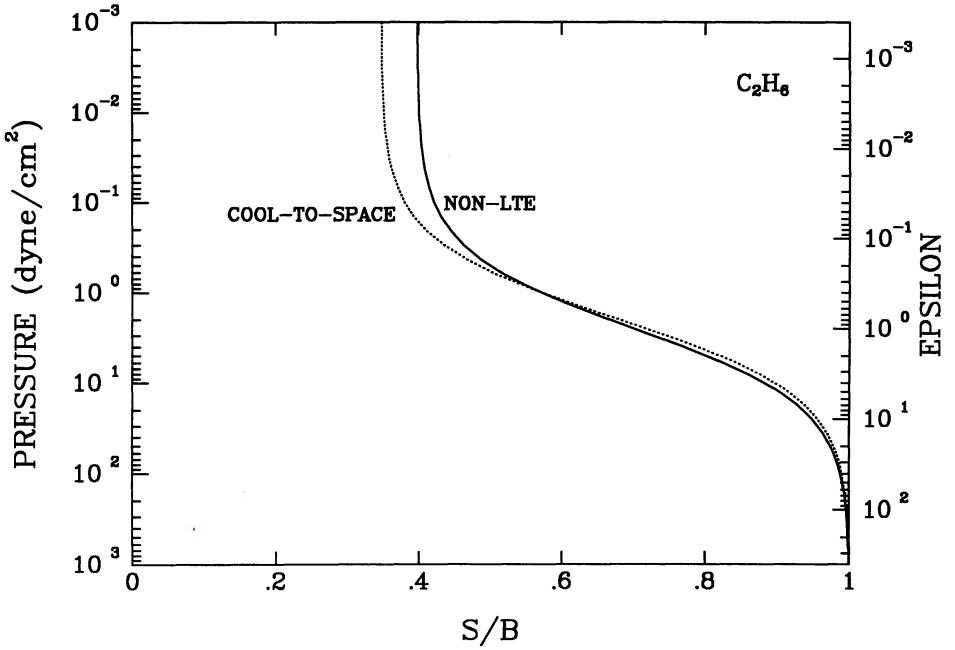

FIG. 11.—Ratio of source function to Planck function for the ν_9 band of C_2H_6. The calculations use a deactivation probability of $P_{10} = 2.1 \times 10^{-5}$. The model atmosphere used in the calculations is isothermal at 175 K with a C_2H_6 mole fraction of 0.01%.

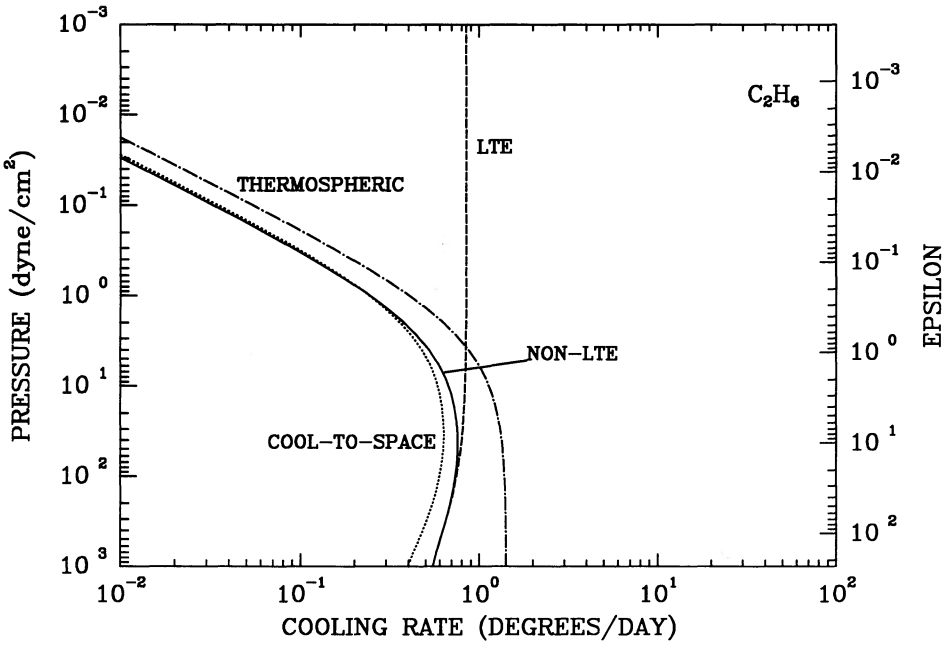

FIG. 12.—Cooling rates for the ν_9 band of C_2H_6. The calculations use a deactivation probability of $P_{10} = 2.1 \times 10^{-5}$. The model atmosphere used in the calculations is isothermal at 175 K with a C_2H_6 mole fraction of 0.01%.

species are temperature dependent. This coupling is ignored in the present work and it is assumed that the Yung and Allen calculations give a good estimate of the mixing ratios at a given pressure despite the fact that the calculated thermal structures differ significantly from the Lellouch et al. (1990) model. Investigation of the effects of thermal structure on composition may be an interesting topic for future applications of this model.

The effects of composition, de-excitation probabilities, and aerosol heating rates on the thermal structure are determined by examining a suite of models obtained by systematic variation of the input parameters. The model parameters are listed in Table 3 and the temperature profiles are shown in Figure 14. The reference model (A) uses the estimated values for de-excitation probabilities at 175 K from Table 2, the Yung and Allen model composition, except for HCN which is scaled by 1/2, and no aerosol heating. The remaining nine models are obtained by scaling the Yung and Allen mixing ratios, by varying collisional de-excitation probabilities, and by including aerosol heating.

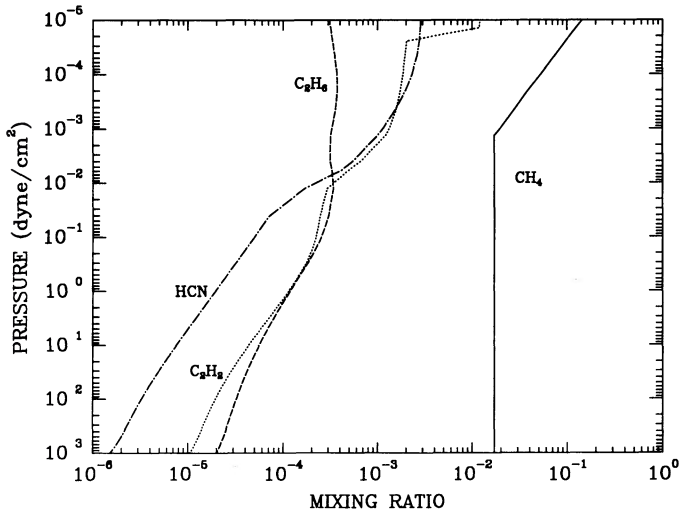

FIG. 13.—Mixing ratios of thermally active species used in the thermal structure calculations (Yung et al. 1984, updated by J. P. Allen & Y. L. Yung 1989, private communication).

The observed thermospheric temperature of 180 ± 20 K is reproduced by all models. The predicted temperatures are much lower than those calculated by Lellouch et al. (1990, see their Fig. 4) because of cooling by HCN, the importance of which was unrecognized in previous studies. Figure 15 shows the contribution to the energy balance equation in the upper thermosphere for model A. Cooling by C_2H_2, CH_4, and C_2H_6 decreases rapidly with altitude because the collisional deactivation rates become small. The cooling rate for these molecules is basically proportional to the pressure squared, as pointed out by Lellouch et al. (1990). HCN cooling, on the other hand, decreases with altitude much less rapidly. This is because the HCN cooling is through rotational transitions, which are in LTE throughout the thermosphere; consequently, the HCN cooling rate tends to be proportional to the pressure. Another noteworthy aspect of this result is that thermal conduction is of minor importance compared to UV heating and HCN cooling. In this regard the thermosphere of Titan is similar to Venus where thermal conduction also plays a relatively minor role (Dickinson & Bougher 1986).

The thermal structure in the mesosphere also differs significantly from the Lellouch et al. (1990) empirical model. In all model runs the mesopause occurs 0.1 μbar, or $\sim$585 km, while the Lellouch et al. (1990) model has a mesopause at 6×10^{-3} μbar, near 800 km. Figure 16 shows the contributions to the net heating rate in the mesosphere and lower thermosphere, from 300 to 700 km, for model A. HCN cooling is weak in this region because the HCN mole fraction decreases drastically below 700 km in the Yung and Allen models and because the rotational lines have become very optically thick and few photons escape to space. Near the lower boundary C_2H_6 is the dominant coolant despite its relatively weak band strength

TABLE 3

MODEL PARAMETERS

MODEL	$P_{10}(10^{-6})$			SCALE FACTORS			AEROSOL HEATING (ergs cm^{-3} s^{-1})
	CH_4	C_2H_2	C_2H_6	C_2H_2	C_2H_6	HCN	
A	1.4	21	21	1.0	1.0	0.5	0.
B	5	125	125	1.0	1.0	0.5	0.
C	1.4	21	100	1.0	1.0	0.5	0.
D	1.4	21	21	2.0	1.0	0.5	0.
E	1.4	21	21	0.5	2.0	0.5	0.
F	1.4	21	21	1.0	1.0	1.0	0.
G	1.4	21	21	1.0	2.0	0.5	0.
H	1.4	21	21	1.0	0.5	0.5	0.
I	1.4	21	21	1.0	1.0	0.5	1×10^{-6}
J	1.4	21	21	1.0	1.0	0.5	5×10^{-6}
K	1.4	21	21	1.0	1.0	0.5	10×10^{-6}
X	Lellouch et al. 1990 model						

compared with C_2H_2, and low abundance compared with CH_4. The reason is that both C_2H_2 and CH_4 are very optically thick and few photons emitted by those molecules can travel to other regions of the atmosphere, while photons emitted by C_2H_6 can escape freely to space. The C_2H_6 cooling at the base of the model causes a negative temperature gradient. The lapse rate at the lower boundary of model A is 0.1 K km^{-1}, while the adiabatic lapse rate is 0.87 K km^{-1} implying that the atmosphere is statically stable. The low temperatures resulting from C_2H_6 cooling cause CH_4 and C_2H_2 to be sources of heat. At these low altitudes (300–350 km) CH_4 and C_2H_2 exchange radiation primarily with the lower boundary, which is relatively warm, partially offsetting the tendency for C_2H_6 to cool the atmosphere.

At ~330 km C_2H_2 becomes a coolant because of the increased probability for photons to escape to space. CH_4 because of its greater abundance is still a source of heat. The lapse rate in this region is roughly 0.06 K km^{-1}. The decrease in temperature is more rapid than would be caused by C_2H_6 alone and at approximately 350 km C_2H_6 becomes a source of heat. At this level C_2H_6, because of its low optical depth, is able to absorb warm radiation from the lower boundary and remains a heat source until ~700 km. The mesopause occurs at 585 km with a temperature of 137.5 K in model A. C_2H_6 is the primary heating agent at the mesopause with a rate 2.2 times larger than solar IR heating and 1.9 times larger than solar UV heating. At higher altitudes all three hydrocarbons become coolants because of elevated temperatures in the ther-

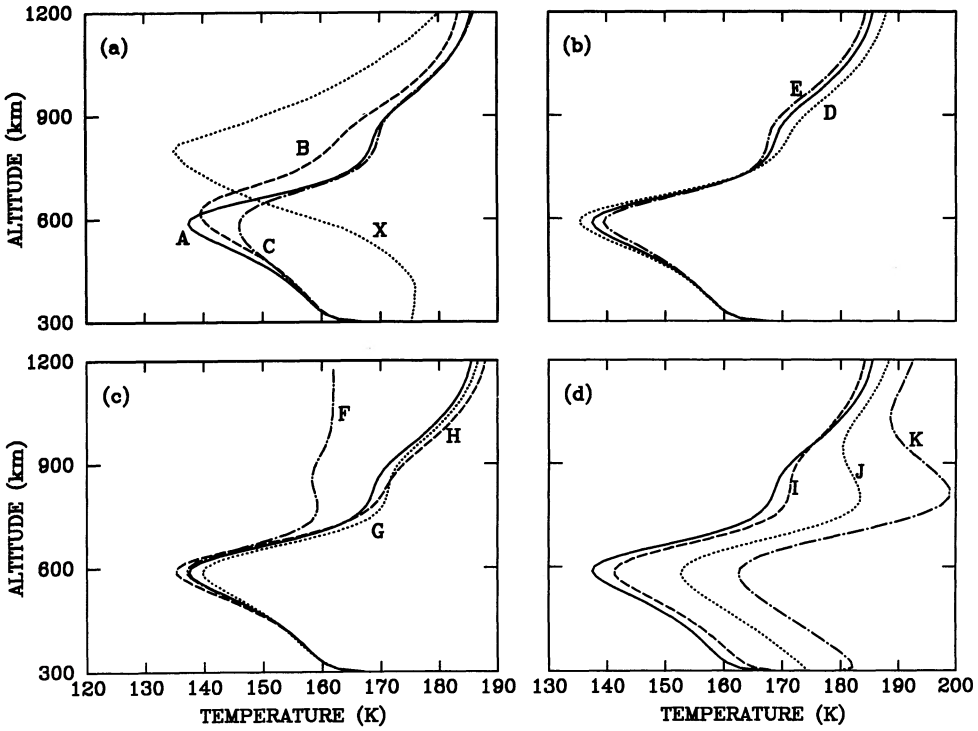

FIG. 14.—Calculated temperature profiles for Titan's atmosphere for a variety of model assumptions. The input parameters for each model are listed in Table 3. The upper left panel (*a*) shows the effect of varying the de-excitation probability. The upper right panel (*b*) shows the effect of varying the C_2H_2 abundance. The lower left panel (*c*) shows the effect of varying the C_2H_6 and HCN abundance. The lower right panel (*d*) shows the effect of aerosol heating.

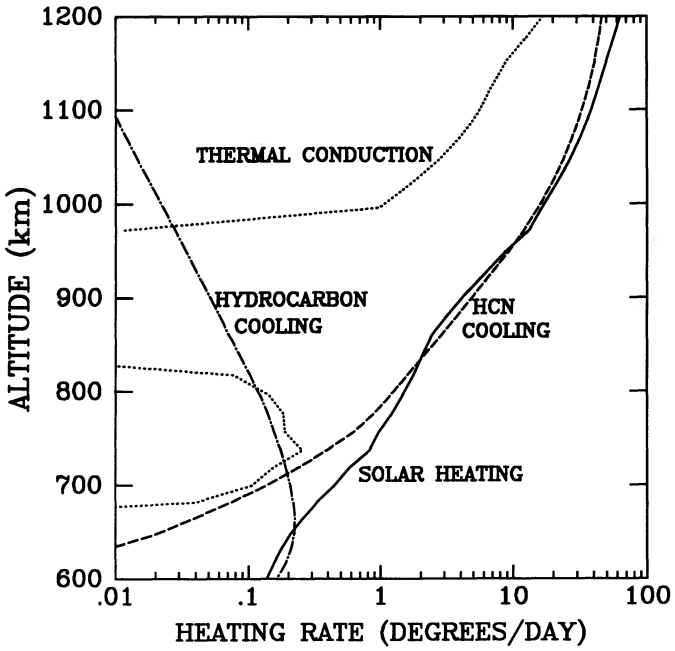

FIG. 15.—Important terms in thermospheric energy balance equation for model A. Above 900 km the thermal structure is determined by UV heating and HCN cooling. The difference between these two curves is due to thermal conduction.

mosphere and the transparency of the atmosphere. The importance of C_2H_6 heating is one of the more surprising results of this study. Previous work has either ignored C_2H_6 or, by neglecting radiative transfer, implicitly assumed that it must function as a coolant. Near the mesopause the atmosphere is cooled primarily by CH_4. This result differs from previous studies (Lellouch et al. 1990; Friedson & Yung 1984) which found that C_2H_2 was the primary coolant.

It is worthwhile to review the reason for the differences between these calculations and earlier work. The low temperatures in the thermosphere found here, which now agree with measurements, are a direct result of HCN cooling. The

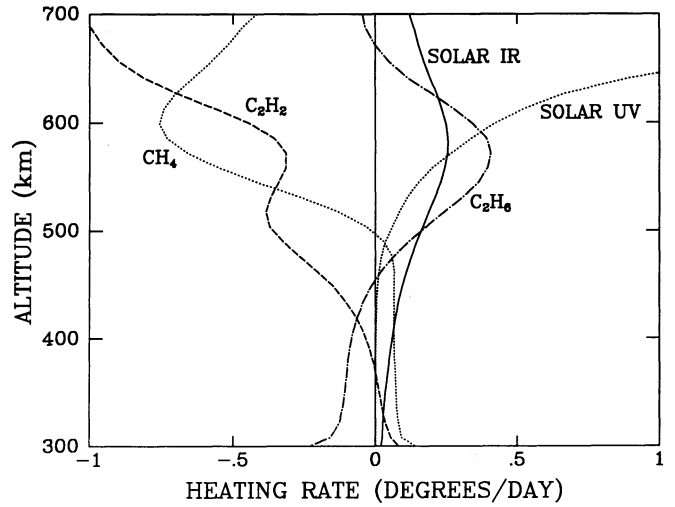

FIG. 16.—Important terms in the mesospheric energy balance for model A. Near the mesopause at 600 km C_2H_6 is the dominant heat source and CH_4 the dominant coolant.

sophisticated radiative transfer employed in these calculations plays a small role in this region of the atmosphere; thus, this result could be found with the simpler thermospheric approximation. As discussed above the thermospheric approximation could be off by ~50% but our knowledge of the HCN abundance is uncertain by this amount. On the other hand, the temperature structure near the mesopause depends critically on the radiative transfer. The large differences between the results reported here and earlier work, which found the mesopause to be much colder and at lower pressures is a direct result of the radiative transfer treatment. In particular, the thermospheric approximation is only capable of dealing with radiative cooling and consequently cannot be used to model C_2H_6 as a heat source. This is the basic reason that the thermospheric approximation, when used in the earlier work by Friedson & Yung (1984) and Lellouch et al. (1990), predicted a much cooler mesopause temperature.

The dependence of thermal structure on the collisional de-excitation rates is shown in Figure 14*a*. Room temperature values (model B) predict differences of only ~2 K from the standard (model A) values near the mesopause, with larger 5–10 K differences at higher altitudes. Larger discrepancies, of roughly 10 K, in the mesopause temperature appear when only the C_2H_6 de-excitation probability is enhanced as in model C. The sensitivity of mesopause temperature on the C_2H_6 de-excitation probability is important because this quantity is poorly known. Clearly, more accurate information on the vibrational relaxation of C_2H_6 is needed to further our understanding of the mesospheric structure on Titan. Similar comments may well apply to the mesospheres of other atmospheres in the outer solar system.

Figure 14*b* illustrates the effects of varying the C_2H_2 abundance. Doubling (halving) the C_2H_2 abundance causes a 2 K decrease (increase) in the mesopause temperature. The small differences in thermospheric structure shown in Figure 14*b* are misleading and are caused by the fact that the temperatures are plotted as a function of altitude rather than pressure. The difference in mesopause temperatures causes an altitude shift which appears as a difference in temperature at higher altitudes. When plotted as a function of pressure the thermal structures are nearly identical, as they should be since C_2H_2 plays a very minor role in determining the thermospheric structure.

The effects of varying the C_2H_6 and HCN mole fractions are shown in Figure 14*c*. Increasing the HCN abundance in model A by a factor of 2 yields model F. The exospheric temperature is 25 K lower and the mesopause temperature is nearly identical. Increasing the C_2H_6 abundance by a factor of 2 produces model G which is ~2 K warmer than model A at the mesopause but is nearly identical otherwise. Model H has a C_2H_6 abundance half as large as model A and is roughly 5 K cooler at the mesopause. Again the thermospheric structure is nearly identical. Thus, the HCN abundance affects primarily the thermospheric structure while the C_2H_6 abundance affects primarily the mesopause structure.

Figure 14*d* shows calculations with aerosol heating. Table 3 lists the aerosol heating rate at 0.1 mbar for these models. The heating rate is assumed to be proportional to the atmospheric pressure and independent of other parameters in the calculation. Aerosol cooling is neglected under the assumption that the particles are small and so radiate inefficiently in the infrared. The rates considered here are based on the analysis of Rages & Pollack (1983) who determine a total extinction at 0.1

mbar of 10^{-4} km $^{-1}$. Assuming that half of the extinction is due to absorption rather than scattering implies a heating rate of $\sim 4 \times 10^{-6}$ ergs cm^{-3} s^{-1}. However, the aerosol opacity varies considerably over Titan while the relative importance of absorption and scattering are not well-known; thus, the aerosol heating rate is very uncertain. Models J and K are 15 and 25 K warmer than model A in the mesosphere and roughly 5 and 10 K warmer in the thermosphere. The change in thermospheric temperature is not due to aerosol heating directly but rather is due to the radiative transfer between hydrocarbons in the warmer mesosphere and the thermosphere.

9.3. *Comparison with Data*

All of the models match the exospheric temperature of 180 ± 20 K, although model F only marginally. The agreement between models and observations is heartening, but the real point is that the temperature structure of the upper thermosphere is controlled by the HCN abundance, provided that the mole fraction is of the order calculated by Yung et al. (1984). It may be possible to further test this result through measurements of the HCN with the Cassini spacecraft. The importance of HCN cooling has other implications which need to be explored. According to the *Voyager* IRIS measurements (Coustenis et al. 1991), the HCN mole fraction in the stratosphere shows a mild increase with latitude. If this tendency persists in the thermosphere then latitudinal variations of solar insolation imply the possibility of interesting dynamics forced by the variation of radiative equilibrium temperature.

From a theoretical point of view the most serious deficiency of the thermospheric portion of the models are the simplistic estimates of the heating efficiencies. More sophisticated heating efficiency calculations require modeling the ionospheric chemistry and are beyond the scope of this work, though sorely needed.

Information on the temperature structure of Titan's atmosphere at intermediate pressures is available from recent ground-based observations of Titan's occultation of 28 Sagittarii. Analysis of the data implies a temperature of $\sim 183 \pm 11$ K at a pressure of 5.1 μbar and an altitude of 450 km (Hubbard et al. 1990; Sicardy et al. 1990). This is more than 30 K warmer than model A but is consistent with model K. However, the occultation analyses assume an isothermal atmosphere while the models possess a negative temperature gradient at the relevant levels. The presence of a temperature gradient may have substantial effects on the derived temperature (see Hubbard, Yelle, & Lunine 1990) with negative gradients causing elevated retrieved temperatures. Detailed comparison between these models and the stellar occultation data is deferred to a later publication.

Smith et al. (1982) inferred an average temperature of 165 K between 200 and 1265 km, from densities measured by the *Voyager* UVS and radio occultation experiments and hydrostatic equilibrium. In the calculations presented here the temperature and pressure at the lower boundary are specified so the agreement between these models and this average temperature can be tested by comparison of the pressures at the upper boundary. With a slight extrapolation the UVS result implies a pressure of 10^{-2} nbar at 1235 km. Model A predicts that the 10^{-2} nbar pressure level occurs at 1236 km and consequently matches the average temperature exactly. The other models are also in excellent agreement with the mean temperature with the exception of model F which is far too cold, and models J and K which are far too hot.

9.4. *Relationship to Photochemistry*

Section 9.2 revealed a striking example of the interplay between photochemistry and thermal structure, concerning the abundance of HCN, which merits further discussion. According to Yung et al. (1984) HCN is produced by the following reaction:

$$N(^4S) + CH_3 \rightarrow HCN + H_2 . \quad (R1)$$

More recent laboratory work indicates that HCN may be formed by a two-step process (Marston & Stief 1989), but this difference has little effect on our discussion. $N(^4S)$ is produced by dissociative ionization of N_2 for $\lambda < 780$ Å

$$h\nu + N_2 \rightarrow N^+ + N(^4S) + e \quad (R2)$$

or ionization

$$h\nu + N_2 \rightarrow N_2^+ + e \quad (R3)$$

followed by recombination

$$N_2^+ + e \rightarrow N(^4S) + N(^2D) . \quad (R4)$$

Direct quenching of $N(^2D)$ to $N(^4S)$ by collisions with N_2 is inefficient but $N(^2D)$ may be converted to $N(^4S)$ through

$$N(^2D) + CH_4 \rightarrow NH + CH_3 \quad (R5)$$

followed by

$$NH + H \rightarrow N(^4S) + H_2 , \quad (R6)$$

although this path may be unlikely (Yung et al. 1984).

This reaction scheme illustrates that the HCN abundance in the thermosphere is primarily determined by the dissociation rate of N_2, which is intimately linked to the heating rate because both are caused by absorption of solar EUV radiation. In fact, energy is released in reactions (R1)–(R6) and to a large extent the molecular processes which dissociate N_2 and lead to HCN production also heat the thermosphere. This is the root of the strong coupling between photochemistry and thermal structure in Titan's thermosphere.

Yung et al. (1984) used 1×10^9 cm^{-2} s^{-1} for the downward flux of odd nitrogen, based on a suggestion by Strobel & Shemansky (1982) that interaction of the thermosphere with magnetospheric electrons is comparable in importance to absorption of solar EUV radiation. More recent work has suggested that this conclusion was probably incorrect and that dissociation of N_2 is driven primarily by absorption of solar EUV radiation (D. F. Strobel 1990, private communication). Strobel & Shemansky (1982) estimate column production rates of 2.5×10^8 cm^{-2} s^{-1} for $N(^4S)$ and $N(^2D)$ for the absorption of solar radiation. Thus, the odd nitrogen flux adopted by Yung et al. (1984) is probably a factor of 2 to 4 too high and scaling their calculated densities downward by a factor of 2 is entirely reasonable. However, if significant magnetospheric precipitation were occuring it would increase both the heating rates and the HCN production rates. Because these two processes affect the thermal structure in opposite directions the net effect on the exospheric temperature may be small.

Figure 17 illustrates the effects of varying the HCN mole fraction on the exospheric temperature for solar maximum and minimum conditions. Because production of HCN depends on the existence of two radicals (N and CH_3) the density should vary as the square of the solar flux. The heating rates from the solar spectra used to represent maximum and minimum condition in Figure 17 differ by a factor of 2.6, which should also

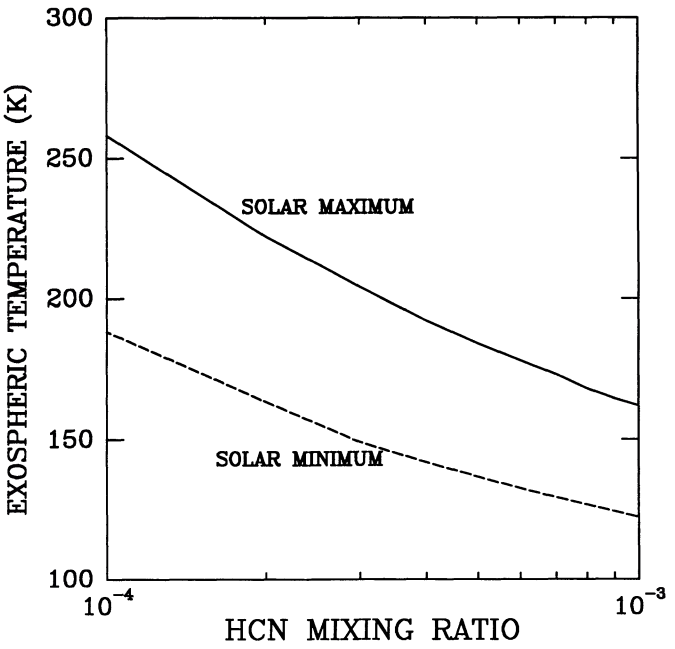

FIG. 17.—Variation of exospheric temperature for HCN mole fraction in the upper atmosphere for solar maximum and minimum conditions.

characterize the solar cycle variation of the N density. CH_3, on the other hand, is produced by solar Lyα which varies by a factor of 1.8, implying a factor of 5 variation in the HCN production rate. Therefore, if a mixing ratio of 5×10^{-4} is adopted for solar maximum a mixing ratio of $\sim 1 \times 10^{-4}$ is appropriate for solar minimum. For these conditions Figure 17 shows that the expected exospheric temperature at solar minimum is also close to 180 K. Thus, the variations of exospheric temperature with solar cycle should be mild, a prediction which may be testable during the planned Cassini mission to Saturn.

The variation of exospheric temperature with solar input is important because it controls the size of the atmosphere. A unique feature of Titan is that the extent of the atmosphere is comparable to the surface radius. If the size of the atmosphere were to increase because of elevated exospheric temperatures Titan would intercept more solar photons and column integrated photolysis rates would increase. Allen et al. (1980) have suggested solar cycle variations in the abundance of hazes because of this effect. The calculations presented here suggest that it does not occur or is at least tempered by the HCN thermostat.

10. SUMMARY

The main conclusion of this work can be summarized as follows:

1. The thermospheric structure is controlled by EUV heating and cooling in the rotational lines of HCN. HCN abundances close to those predicted by Yung et al. (1984) yield exospheric temperatures in agreement with UVS measurements (Smith et al. 1982).

2. Titan should have a cool mesopause with a minimum temperature of ~ 140 K at an altitude of 600 km, where the pressure is 0.1 μbar.

3. The LTE approximation to the source function extends to values of $\epsilon = 0.02$ for CH_4, $\epsilon = 0.05$ for C_2H_2, and $\epsilon = 1$ for C_2H_6.

4. The thermospheric approximation to the cooling rates contains large errors principally because of the small temperature rise in Titan's thermosphere. The LTE approximation works fairly well at high pressure but there are significant deviations from the non-LTE results at surprisingly high pressures (~ 10 μbar). This effect is most pronounced for C_2H_2.

5. C_2H_6 is a critical heating agent in the upper atmosphere because it efficiently absorbs warm stratospheric radiation. C_2H_6 is the primary heating agent at the mesopause and is responsible for the relatively warm temperatures found in this study.

6. The thermal structure is sensitive to collisional deactivation rates, especially for C_2H_6. Further laboratory work in this area is highly desirable.

The author has benefited from discussions with D. Hunten, L. Wallace, B. Bezard, A. Coustenis, E. Lellouch, D. Strobel, D. Crisp, and R. West. Permission to use the updated photochemical models of M. Allen and Y. Yung is gratefully acknowledged. The C_2H_6 line list was generously provided by B. Bezzard and G. Bjorker. This research was supported by NASA grant NAGW-2017.

APPENDIX

The numerical techniques used to calculate non-LTE source functions and heating rates are adopted from the extensive literature on non-LTE processes in stellar atmospheres. Mihalas (1978) presents an excellent review of this field and serves as a useful starting point for this discussion. Because of important differences between radiative transfer in a molecular band and radiative transfer in atomic lines the relevant techniques cannot be borrowed directly from the stellar atmosphere literature but need to be adapted to the problem at hand. The manner in which this is done is described below.

A1. RYBICKI'S METHOD

As mentioned in the main text the computing time required for Rybicki's method scales linearly with the number of frequency integration points and it is ideally suited to radiative transfer in molecular bands. Rybick's method first requires changing variables from specific intensity I_ν to the "Feautrier" variable $\mathcal{J}_\nu$ defined by

$$\mathcal{J}_\nu = \tfrac{1}{2}[\mathcal{J}_\nu(\mu) + \mathcal{J}_\nu(-\mu)] . \tag{A1}$$

The radiative transfer equation becomes

$$\mu^2 \frac{d^2}{d\tau_\nu^2} \mathcal{J}_\nu = \mathcal{J}_\nu - \mathcal{S}_\nu . \tag{A2}$$

To proceed further the atmosphere is divided into ND layers and a superscript (usually d) is used to denote the value of a function (i.e., intensities, sources, functions, etc.) in a particular layer. It is convenient to denote frequencies and angles with a single subscript, thus $\mathscr{I}_i^d$ represents the specific intensity in layer d at frequency-angle i. For NF frequency points and NU angular integration points, i will range from 1 to NI = NF × NU. Bold face letters are used to represent column vectors whose elements are the value of the function in each atmospheric layer. With these definitions the discrete form of equation (A2) can be written as

$$\boldsymbol{M}_i \boldsymbol{J}_i = \boldsymbol{S}_i \,, \tag{A3}$$

where the $\boldsymbol{J}_i$ and $\boldsymbol{S}_i$ are column vectors whose elements are the values of the functions $\mathscr{J}_\nu(z, \mu)$ and $\mathscr{S}_\nu(z, \mu)$ in each atmospheric layer. The quantity $\boldsymbol{M}_i$ is the discrete form of the differential operator $1 - \mu^2 d/d\tau_\nu^2$. Replacing derivatives by differences gives

$$\begin{aligned} M_i^{d,d-1} &= -\frac{\mu_i^2}{\Delta\tau_i^d \Delta\tau_i^{d-1/2}} \,, \\ M_i^{d,d} &= 1 - \frac{\mu_i^2}{\Delta\tau_i^d}\left(\frac{1}{\Delta\tau_i^{d-1/2}} + \frac{1}{\Delta\tau_i^{d+1/2}}\right), \\ M_i^{d,d+1} &= -\frac{\mu_i^2}{\Delta\tau_i^d \Delta\tau_i^{d+1/2}} \,, \end{aligned} \tag{A4}$$

where

$$\begin{aligned} \Delta\tau_i^{d\pm 1/2} &= \mp\tau_i^d \pm \tau_i^{d\pm 1} \\ \Delta\tau_i^d &= \tfrac{1}{2}(\Delta\tau_i^{d+1/2} + \Delta\tau_i^{d-1/2}) \end{aligned} \tag{A5}$$

The definition of mean intensity (eq. [5]) becomes in matrix form

$$\boldsymbol{I} = \sum_{i=1}^{\mathrm{NI}} \boldsymbol{W}_i \boldsymbol{J}_i \,, \tag{A6}$$

where $\boldsymbol{W}_i$ is an ND × ND diagonal matrix containing the product of frequency and angular weights for the integration. Expressing the source function in terms of mean intensity and the Planck function through equation (10) yields the formal solution of the radiative transfer equation

$$\boldsymbol{J}_i = \boldsymbol{M}_i^{-1} \boldsymbol{U}_i \boldsymbol{I} + \boldsymbol{M}_i^{-1} \boldsymbol{K}_i \,, \tag{A7}$$

where elements of the vector $\boldsymbol{K}_i$ are given by

$$K_i^d = \epsilon^d \mathscr{B}_i^d / (1 + \epsilon^d) \,. \tag{A8}$$

and the diagonal matrix $\boldsymbol{U}_i$ by

$$U_i^{d,d} = \mathscr{B}_i^d / \mathscr{B}^d (1 + \epsilon^d) \,. \tag{A9}$$

Multiplication of equation (A7) by $\boldsymbol{W}_i$, summation over frequency-angle points, and substitution of (A6) gives

$$\left(1 - \sum_{i=1}^{\mathrm{NI}} \boldsymbol{W}_i \boldsymbol{M}_i^{-1} \boldsymbol{U}_i\right) \boldsymbol{I} = -\sum_{i=1}^{\mathrm{NI}} \boldsymbol{W}_i \boldsymbol{M}_i^{-1} \boldsymbol{K}_i \,, \tag{A10}$$

The radiative transfer equation has been reduced to a matrix equation of dimension ND. It is worth emphasizing that use of this technique depends on the fact that the rotational levels of the upper vibrational state are in LTE.

Solution of the radiative transfer equation with this adaptation of Rybicki's method is reminiscent of the Curtis matrix approach used in the calculations of Curtis & Goody (1956) and more recently by Lopez-Puertas et al. (1986) and the exchange integrals discussed by Dickinson (1972). The only difference appears in the way that the matrix elements are calculated. In the usual implementation of the Curtis matrix approach the matrix elements are calculated as second derivatives of the transmission function while Rybicki's technique calculates the matrix elements through discretization of the differential form of the radiative transfer equation. The relative merits of the integral (Curtis matrix) and differential (Rybicki) techniques are discussed at length in Mihalas (1978), who strongly recommends the differential equation approach. One immediate advantage of the differential equation approach is the relative ease with which derivatives of heating rates with respect to temperature can be calculated. These derivatives are directly related to the radiative cooling time constants and can be used to find steady state solutions for the thermal structure.

A2. TEMPERATURE DERIVATIVES

A generalized Newton-Raphson method is used to calculate temperature profiles. This approach requires calculation of the derivative of the radiative heating rate with respect to temperature. Taking the temperature derivative of the radiative transfer equation (A3) yields

$$\boldsymbol{M}_i \dot{\boldsymbol{J}}_i + \boldsymbol{V}_i = \boldsymbol{U}_i \dot{\boldsymbol{I}} + \dot{\boldsymbol{U}}_i \boldsymbol{I} + \dot{\boldsymbol{K}}_i \tag{A11}$$

where the dots represent derivatives with respect to temperature. $\dot{\boldsymbol{K}}_i$ is a diagonal matrix with elements given by

$$\dot{K}_i^{d,d} = \frac{\partial}{\partial T}\left(\frac{\epsilon \mathscr{B}_i}{1+\epsilon}\right)\bigg|_{T=T^d}. \tag{A12}$$

The matrix $\dot{\boldsymbol{U}}_i$ is also diagonal with elements

$$\dot{U}_i^{d,d} = \frac{\partial}{\partial T}\left(\frac{\mathscr{B}_i}{\mathscr{B}(1+\epsilon)}\right)\bigg|_{T=T^d}. \tag{A13}$$

The matrix $\boldsymbol{V}_i$ is tridiagonal with components

$$V_i^{d,d-1} = \frac{\mu_i^2}{\Delta\tau_i^{d-1/2}}\frac{\partial \Delta\tau_i^{d-1/2}}{\partial T^{d-1}}\left[\frac{J_i^{d-1}-J_i^d}{\Delta\tau_i^{d-1/2}\Delta\tau_i^d}+\frac{1}{2}\frac{\Delta\tau^{d-1/2}}{\Delta\tau_i^d}\left(\frac{J_i^{d-1}-J_i^d}{\Delta\tau_i^{d-1/2}\Delta\tau_i^d}+\frac{J_i^{d+1}-J_i^d}{\Delta\tau_i^{d+1/2}\Delta\tau_i^d}\right)\right],$$

$$V_i^{d,d} = \frac{\mu_i^2}{\Delta\tau_i^{d-1/2}}\frac{\partial \Delta\tau_i^{d-1/2}}{\partial T^{d}}\left[\frac{J_i^{d-1}-J_i^d}{\Delta\tau_i^{d-1/2}\Delta\tau_i^d}+\frac{1}{2}\frac{\Delta\tau^{d-1/2}}{\Delta\tau_i^d}\left(\frac{J_i^{d-1}-J_i^d}{\Delta\tau_i^{d-1/2}\Delta\tau_i^d}+\frac{J_i^{d+1}-J_i^d}{\Delta\tau_i^{d+1/2}\Delta\tau_i^d}\right)\right]$$
$$+\frac{\mu_i^2}{\Delta\tau_i^{d+1/2}}\frac{\partial \Delta\tau_i^{d+1/2}}{\partial T^{d}}\left[\frac{J_i^{d+1}-J_i^d}{\Delta\tau_i^{d+1/2}\Delta\tau_i^d}+\frac{1}{2}\frac{\Delta\tau_i^{d+1/2}}{\Delta\tau_i^d}\left(\frac{J_i^{d-1}-J_i^d}{\Delta\tau_i^{d-1/2}\Delta\tau_i^d}+\frac{J_i^{d+1}-J_i^d}{\Delta\tau_i^{d+1/2}\Delta\tau_i^d}\right)\right],$$

$$V_i^{d,d+1} = \frac{\mu_1^2}{\Delta\tau_i^{d+1/2}}\frac{\partial \Delta\tau_i^{d+1/2}}{\partial T^{d+1}}\left[\frac{J_i^{d+1}-J_i^d}{\Delta\tau_i^{d+1/2}\Delta\tau_i^d}+\frac{1}{2}\frac{\Delta\tau_i^{d+1/2}}{\Delta\tau_i^d}\left(\frac{J_i^{d-1}-J_i^d}{\Delta\tau_i^{d-1/2}\Delta\tau_i^d}+\frac{J_i^{d+1}-J_i^d}{\Delta\tau_i^{d+1/2}\Delta\tau_i^d}\right)\right]. \tag{A14}$$

Taking the temperature derivative of equation (A6) yields

$$\dot{\boldsymbol{I}} = \sum_{i=1}^{\mathrm{NI}}(\boldsymbol{W}_i\dot{\boldsymbol{J}}_i + \dot{\boldsymbol{W}}_i\boldsymbol{J}_i), \tag{A15}$$

where

$$\dot{W}_i^{d,d} = \frac{\partial}{\partial T}W_i\bigg|_{T=T^d}. \tag{A16}$$

Solving (A11) for $\dot{\boldsymbol{J}}_i$, multiplying the results by $\boldsymbol{W}_i$, summing over i, and substitution into (A14) yields

$$\left(1-\sum_{i=1}^{\mathrm{NI}}\boldsymbol{W}_i\boldsymbol{M}_i^{-1}\boldsymbol{U}_i\right)\dot{\boldsymbol{I}} = \sum_{i=1}^{\mathrm{NI}}[\boldsymbol{W}_i\boldsymbol{M}_i^{-1}(\dot{\boldsymbol{U}}_i\boldsymbol{I}+\dot{\boldsymbol{K}}_i-\boldsymbol{V}_i)+\dot{\boldsymbol{W}}_i\boldsymbol{J}_i] \tag{A17}$$

which is an ND × ND matrix equation for $\dot{\boldsymbol{I}}$.

Computation of the temperature derivatives of the heating rates by this analytic method is far more efficient than calculation of the derivative as the numerical differences of heating rates. For an atmosphere with ND depth points the heating rate must be calculated ND^2 times to determine the matrix of temperature derivatives. With this analytic scheme the heating rate and its derivative need to be calculated so that computing time is roughly proportional to 2 × ND. Clearly, the analytic technique is preferable if ND is large.

A3. STEADY-STATE SOLUTIONS

Steady-state solutions to the energy balance equation are found by solving equation (36) in the form

$$\boldsymbol{F} \equiv \boldsymbol{R}({}^{m+1}\boldsymbol{T} - {}^{m}\boldsymbol{T}) - \boldsymbol{CT} - \sum_j \boldsymbol{H}_j = 0 \tag{A18}$$

where $\boldsymbol{CT}$ represents the discrete form of the thermal conduction term and $\boldsymbol{R}$ is a diagonal matrix with elements

$$R^d = \frac{\rho^d c_p^d}{\Delta t} \tag{A19}$$

For the calculations presented here the time step, Δt, is set to 10^{12} s. The quantity ${}^{m}\boldsymbol{T}$ represents the array of temperatures at the mth time step. The temperature at the $m+1$ time step is given by

$${}^{m+1}\boldsymbol{T} = {}^{m}\boldsymbol{T} - \dot{\boldsymbol{F}}^{-1}\boldsymbol{F}({}^{m}\boldsymbol{T}). \tag{A20}$$

The quantity $\dot{\boldsymbol{F}}$ depends on the derivative of the heating rate and consequently on $\dot{\boldsymbol{I}}$. The derivative of heating rate at level d with respect to temperature at level k is given by

$$\dot{H}^{d,k} = 4\pi k_o\frac{\epsilon^d}{1+\epsilon^d}\dot{I}^{d,k} + 4\pi k_o\left[(I-\mathscr{B})\frac{\partial}{\partial T}\left(\frac{\epsilon}{1+\epsilon}\right) - \frac{\epsilon}{1+\epsilon}\frac{\partial \mathscr{B}}{\partial T}\right]_{T=T^d}\delta^{d,k}, \tag{A21}$$

where $\delta^{d,k}$ is the Kronecker delta function. Calculation of the derivative of the thermal conduction term is straightforward and will not be reproduced here. The heating rate derivative for HCN cooling may be obtained from equation (A21) by letting $\epsilon \to \infty$.

Solution of the energy balance equation with the combined time stepping/Newton-Raphson approach is convenient because quantities which vary slowly with temperature can be calculated at each time step, rather than in each Newton-Raphson iteration. In the calculations presented here the solar UV and IR heating rates and the hydrostatic equilibrium equation are calculated at each time step while the IR heating rates and thermal conduction term are calculated at each Newton-Raphson iteration. Generally three to five time steps with between two and five Newton-Raphson iterations are sufficient to achieve convergence. It was found that the absorption coefficients must be recalculated during each Newton-Raphson iteration. This is unfortunate because the absorption coefficient calculations are the most time-consuming part of the calculations. A number of schemes were tried where adsorption coefficients were estimated using earlier values derivatives, but all failed dismally.

REFERENCES

Allen, D. C., Scragg, T., & Simpson, C. J. S. M. 1980, Chem. Phys., 51, 279
Allen, M., Pinto, J. P., & Yung, Y. L. 1980, ApJ, 242, L125
Appleby, J. F. 1990, Icarus, 85, 355
Apruzese, J. P., & Strobel, D. F. 1984, J. Geophys. Res., 89, 7187
Chamberlain, J. W. 1962, ApJ, 136, 582
Cotrell, T. L., & McCoubrey, J. C. 1961, Molecular Energy Transfer in Gases (London: Butterworth Scientific Publications)
Coustenis, A., Bezard, B., & Gautier, D. 1989, Icarus, 80, 54
Coustenis, A., Bezard, B., Gautier, D., Marten, A., & Samuelson, R. 1991, Icarus, 89, 152
Curtis, A. R., & Goody, R. M. 1956, Proc. R. Soc., London, A236, 193
Daunt, S. J., Atakan, A. K., Blass, W. E., Halsey, G. W., Jennings, D. E., Reuter, D. C., Susskind, J., & Brault, J. W. 1984, ApJ, 280, 921
Dickinson, R. E. 1972, J. Atmos. Sci., 29, 1531
———. 1975, J. Atmos. Sci., 33, 290
———. 1976, Icarus, 27, 479
———. 1984, J. Atm. Terr. Phys., 46, 995
Dickinson, R. E., & Bougher, S. W. 1986, J. Geophys. Res., 91, 70
Dickinson, R. E., & Ridley, E. C. 1977, Icarus, 30, 163
Friedson, A. J., & Yung, Y. L. 1984, J. Geophys. Res., 89, 85
Goody, R. M., & Yung, Y. L. 1989, Atmospheric Radiation (Oxford: Oxford Univ. Press)
Herzberg, G. 1945, Infrared and Raman Spectra of Polyatomic Molecules (Princeton, NH: Van Nostrand)
Haeger, J., Krieger, W., & Pfab, J. 1981, J. Chem. Soc. Faraday Trans. 2, 77, 469
Haeger, J., Krieger, W., Ruegg, T., & Walther, H. 1980, J. Chem. Phys., 72, 4286
Hastings, J. T., & Roble, R. G. 1977, Planet. Space Sci., 25, 209
Hesse, P., & Moore, C. B. 1976, J. Chem. Phys., 65, 2339
Hess, P., Kung, A. H., & Moore, C. B. 1980, J. Chem. Phys., 72, 5525
Houghton, J. T. 1969, QJRAS, 95, 1
———. 1986, The Physics of Atmospheres (Cambridge: Cambridge Univ. Press)
Hubbard, W., Hunten, D. M., Reitsema, H. J., Brosch, N., Nevo, Y., Carreira, E., Rossi, F., & Wasserman, L. H. 1990, Nature, 343, 353
Hubbard, W. B., Yelle, R. V., & Lunine, J. I. 1990, Icarus, 84, 1
Husson, N., et al. 1986, Ann. Geophys., 4, 185
Kostriuk, T., Espenak, F., Romani, P., Zipoy, D., & Goldstein, J. 1990, Icarus, 88, 87
Kuhn, W. R., & London, J. 1969, J. Atmos. Sci., 26, 189
Kutepov, A. A., & Shved, G. M. 1978, Izv. Atmos. Oceanic Phys., 14, 18
Lambert, J. D., & Salter, R. 1959, Proc. R. Soc., London A, 253, 277
Landau, L., & Teller, E. 1936, Phys. Z., 10, 34
Lellouch, E., Coustenis, A., Gautier, D., Raulin, F., Dubouloz, N., & Frere, C. 1989, Icarus, 79, 328
Lellouch, E., Hunten, D. M., Kockarts, G., & Coustenis, A. 1990, Icarus, 83, 308
Lopez-Puertas, M., Rodrigo, R., Molina, A., & Taylor, F. W. 1986, J. Atm. Terr. Phys., 48, 729
Marston, G., & Stief, L. J. 1989, Res. Chem. Intermed., 12, 161
McKay, C. P., Pollack, J. B., & Courtin, R. 1989, Icarus, 80, 23
Mihalas, D. 1978, Stellar Atmospheres, 2nd ed. (New York: Freeman)
Moore, C. B. 1965, J. Chem. Phys., 43, 2979
Mount, G. H., & Rottman, G. L. 1981, J. Geophys. Res., 86, 9193
Rages, K., & Pollack, J. 1983, Icarus, 55, 50
Samuelson, R. E. 1983, Icarus, 53, 364
Schwartz, R. N., Slawsky, Z. I., & Herzfeld, K. F. 1952, J. Chem. Phys., 20, 1591 (SSH)
Shved, G. M. 1974, AZh, 18, 499
Sicardy, B., et al. 1990, Nature, 343, 350
Smith, G. R., Strobel, D. F., Broadfoot, A. L., Sandel, B. R., Shemansky, D. E., & Holberg, J. B. 1982, J. Geophys. Res., 87, 1351
Smith, N. J. G., David, C. C., & Smith, I. W. M. 1985, J. Chem. Soc. Faraday Trans. 2, 81, 417
Strobel, D. E., Meier, R. R., Summers, M. E., & Strickland, D. J. 1991, Geophys. Res. Lett., in press
Strobel, D. E., & Shemansky, D. E. 1982, J. Geophys. Res., 87, 1361
Strobel, D. F., & Smith, G. R. 1973, J. Atmos. Sci., 30, 718
Torr, M. R., & Torr, D. G. 1985, J. Geophys. Res., 90, 6675
Valley, L. M., & Levgold, S. 1960, Phys. Rev. Lett., 4, 627
Wang, J. C. F., & Springer, G. S. 1977, Prog. Astronaut. Aeronaut., 51, 849
West, R., Chen, L., & Crisp, D. 1990, J. Quant. Spectrosc. Rad. Transf., 43, 191
Yardley, J. T., Fertig, M. N., & Moore, C. B. 1970, J. Chem. Phys., 52, 1450
Yardley, J. T., & Moore, C. B. 1968, J. Chem. Phys., 49, 1111
Yelle, R. V., & Lunine, J. I. 1989, Nature, 33, 288
Yuan, R. C., Press, J. M., Flynn, G. W., & Ronn, A. M. 1973, J. Chem. Phys., 59, 6128
Yung, Y. L., Allen, M., & Pinto, J. P. 1984, ApJ, 55, 465
Zittel, P. F., & Moore, C. B. 1973, J. Chem. Phys., 58, 2004